J|A|C|S
ARTICLES
Published on Web 03/17/2004

Marked Counteranion Effects on Single-Site Olefin Polymerization Processes. Correlations of Ion Pair Structure and Dynamics with Polymerization Activity, Chain Transfer, and Syndioselectivity

Ming-Chou Chen, John A. S. Roberts, and Tobin J. Marks*

Contribution from the Department of Chemistry, Northwestern University, Evanston, Illinois 60208-3113

Received May 22, 2003; E-mail: tjmarks@casbah.acns.nwu.edu

Abstract: Counteranion effects on the rate and stereochemistry of syndiotactic propylene enchainment by the archetypal C_s-symmetric precatalyst $[Me_2C(Cp)(Flu)]ZrMe_2$ (**1**; Cp = C_5H_4; Flu = $C_{13}H_8$, fluorenyl) are probed using the cocatalysts MAO (**2**), $B(C_6F_5)_3$ (**3**), $B(2\text{-}C_6F_5C_6F_4)_3$ (**4**), $Ph_3C^+B(C_6F_5)_4^-$ (**5**), and Ph_3C^+-$FAl(2\text{-}C_6F_5C_6F_4)_3^-$ (**6**), offering greatly different structural and ion pairing characteristics. Reaction of **1** with **3** affords $[Me_2C(Cp)(Flu)]ZrMe^+$ $MeB(C_6F_5)_3^-$ (**7**). In the case of **4**, this reaction leads to formation the μ-methyl dinuclear diastereomers $\{([Me_2C(Cp)(Flu)]ZrMe)_2(\mu\text{-}Me)\}^+$ $MeB(2\text{-}C_6F_5C_6F_4)_3^-$ (**8**). A similar reaction with **6** results in diastereomeric $[Me_2C(Cp)(Flu)]ZrMe^+$ $FAl(2\text{-}C_6F_5C_6F_4)_3^-$ (**10**) ion pairs. The molecular structures of **7** and **10** have been determined by single-crystal X-ray diffraction. Reorganization pathways available to these species have been examined using EXSY and dynamic NMR, revealing that the cation-$MeB(C_6F_5)_3^-$ interaction is considerably weaker/more mobile than in the $FAl(2\text{-}C_6F_5C_6F_4)_3^-$-derived analogue. Polymerizations mediated by **1** in toluene over the temperature range of −10° to +60 °C and at 1.0−5.0 atm propylene pressure (at 60 °C) reveal that activity, product syndiotacticity, *m* and *mm* stereodefect generation, and chain transfer processes are highly sensitive to the nature of the ion pairing. Thus, the complexes activated with **4** and **5**, having the weakest ion pairing, yield the highest estimated propagation rates, while with **6**, having the strongest pairing, yields the lowest. The strongly coordinating, immobile $FAl(2\text{-}C_6F_5C_6F_4)_3^-$ anion produces the highest/least temperature-dependent product syndiotacticity, lowest/least temperature-dependent *m* stereodefect abundance, and highest product molecular weight. These polypropylene microstructural parameters, and also M_w, are least sensitive to increased propylene pressure for $FAl(2\text{-}C_6F_5C_6F_4)_3^-$, but highest with $MeB(C_6F_5)_3^-$. In general, *mm* stereodefect production is only modestly anion-sensitive; [propylene] dependence studies reveal enantiofacial propylene misinsertion to be the prevailing *mm*-generating process in all systems at 60 °C, being most dominant with **6**, where *mm* stereodefect abundance is lowest. For 1,3-dichlorobenzene as the polymerization solvent, product syndiotacticity, as well as *m* and *mm* stereodefects, become indistinguishable for all cocatalysts. These observations are consistent with a scenario in which ion pairing modulates the rates of stereodefect generating processes relative to monomer enchainment, hence net enchainment syndioselectivity, and also dictates the rate of termination relative to propagation and the preferred termination pathway. In comparison to **3**−**6**, propylene polymerization mediated by MAO (**2**) + **1** in toluene reveals an estimated ordering in site epimerization rates as **5** > **4** > **2** > **3** > **6**, while product syndiotacticities rank as **6** > **2** > **5** ∼ **4** > **3**.

Introduction

Cocatalysts are of great current interest as vital components of single-site olefin polymerization catalysts.[1,2] Well-known cocatalysts include methylaluminoxane (MAO; **2**),[3] tris(perfluorophenyl)borane $B(C_6F_5)_3$; (**3**),[4] and related perfluoroarylboranes,[5] ammonium or trityl salts of $B(C_6F_5)_4^-$ (**5**)[6] and related perfluoroarylborates,[7] and aluminates,[8] all of which undergo reaction with metallocenes to generate highly active "cationic" complexes as the actual agents for olefin polymerization (**A**; eq 1). Over the past two decades, numerous elegant efforts have

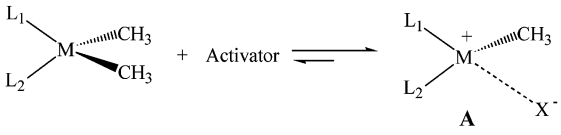

(1)

been directed at "engineering" the cationic portion of such catalysts,[1c] however only recently has the charge-compensating anion (X^-) begun to receive attention in regard to understanding

(1) For recent reviews, see: (a) Pédeutour, J.-N.; Radhakrishnan, K.; Cramail, H.; Deffieux, A. *Macromol. Rapid Commun.* **2001**, *22*, 1095−1123. (b) Chen, Y.-X.; Marks, T. J. *Chem. Rev.* **2000**, *100* (4), 1391−1434. (c) Gladysz, J. A., Ed. *Chem. Rev.* **2000**, *100*, 1167−1682. (d) Marks, T. J.; Stevens, J. C., Eds. *Top. Catal.* **1999**, *7*, 1−208. (e) Britovsek, G. J. P.; Gibson, V. C.; Wass, D. F. *Angew. Chem., Int. Ed. Engl.* **1999**, *38*, 428−447. (f) Jordan, R. F.; Ed. *J. Mol. Catal.* **1998**, *128*, 1−337.

and optimizing the role of the ion pairing dynamics in catalyst system performance. Strong evidence now suggests that the activator and the structures of the resulting ion pairs can have a profound influence on single-site polymerization catalyst activity, lifetime, stability, chain-transfer characteristics, and possibly stereoregulation.[1,2] As part of our continuing efforts to characterize cocatalyst-related structure−reactivity relationships for such catalysts, we are particularly interested in fluoroarylborate and -aluminate anions and the ion pairing behavior of complexes derived from them. Recently, we communicated some preliminary observations on counteranion effects on propylene enchainment stereochemistry by the archetypal C_s-symmetric precatalyst $[Me_2C(Cp)(Flu)]ZrMe_2$ (**1**; Cp = C_5H_4; Flu = fluorenyl),[9] using a series of structurally/coordinatively diverse cocatalysts/counteranions.[10] In principle, the established pathway[11] for syndiospecific propylene enchainment by C_s-symmetric catalysts should be a sensitive probe of the importance of cocatalyst/counteranion[1,2] interactions since olefin enchainment must occur in concert with "chain swinging" (eq 2, R = polypropylene fragment). It is known that rates of similar reorganization/symmetrization processes are sensitive to ion pairing strength in model metallocenium systems (R = H, alkyl group),[12] and thought that analogous "back-skip" processes without concomitant enchainment are a major source of polypropylene stereodefects in C_s-symmetric systems (site epimerization, Scheme 1B). These stereodefects, in particular *m*-type stereodefects, have distinct spectroscopic signatures and can be quantified, as has been established.[11,13]

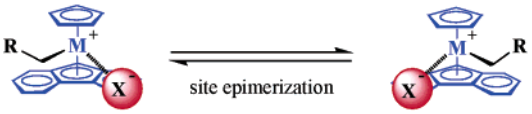

(2)

In the preliminary work,[10] it was observed that counteranion effects are strikingly large, and to a significant degree qualitatively understandable, in terms of established trends in ion pairing strength and dynamics. The results at that stage suggested a mechanistic picture in which anion-specific ion pairing effects modulate not only the enchainment and chain transfer rates, but more importantly, the *relative rates* of enchainment versus *m* stereodefect generation. This suggested that the strong coordinative characteristics of $FAl(2\text{-}C_6F_5C_6F_4)_3^-$ (**B**)[8a,b] lead to more tightly bound, stereochemically immobile ion pairs, accounting both for the decrease in polymerization activity and for the enhancement in stereoselectivity. A solvent effect was also observed: in low-polarity toluene, polymeriza-

B

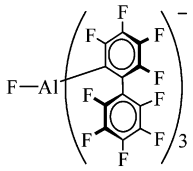

tion activity, product syndiotacticity, and product molecular weight are sensitively dependent on counteranion identity. In contrast, a "leveling effect" on product stereoregularity is observed in polar 1,3-dichlorobenzene, i.e., the anion dependence is strongly attenuated.

These findings and the questions raised by the apparent significance of ion pairing in C_s-symmetric polymerization systems motivate the present broader and more quantitative investigation of solution-phase catalyst structure and dynamics, and correlation of these results with polymerization activity, chain transfer pathways, and tacticity/microstructure, as well as detailed determination of ion pair structures in the solid state. Ion pairing effects are found to manifest themselves differently for different processes occurring during polymerization, allowing nonsystematic effects on directly observable product polymer properties (e.g., on syndiotacticity or average molecular weight) to emerge from *systematic* effects on individual processes (propagation, site epimerization, chain release, etc.).

Furthermore, recent reports of concentration-dependent ion pair aggregation and anion exchange processes in zirconocenium

(2) For recent cocatalyst studies, see: (a) Busico, V.; Cipullo, R.; Cutillo, F.; Vacatello, M.; Van Axel Castelli, V. *Macromolecules* **2003**, *36*, 4258−4261. (b) Mohammed, M.; Nele, M.; Al-Humydi, A.; Xin, S.; Stapleton, R.; Collins, C. *J. Am. Chem. Soc.* **2003**, *125*, 7930−7941. (c) Li, L.; Metz, M. V.; Li, H.; Chen, M.-C.; Marks, T. J. *J. Am. Chem. Soc.* **2002**, *124*, 12 725−12 741. (d) Metz, M. V.; Schwartz, D. J.; Stern, C. L.; Marks, T. J.; Nickias, P. N. *Organometallics* **2002**, *21*, 4159−4168. (e) Metz, M. V.; Sun, Y. M.; Stern, C. L.; Marks, T. J. *Organometallics* **2002**, *21*, 3691−3702. (f) Wilmes, G. M.; Polse, J. L.; Waymouth, R. M. *Macromolecules* **2002**, *35*, 6766−6772. (g) Lancaster, S. J.; Rodriguez, A.; Lara-Sanchez, A.; Hannant, M. D.; Walker, D. A.; Hughes, D. H.; Bochmann, M. *Organometallics* **2002**, *21*, 451−453. (h) Rodriguez, G.; Brant, P. *Organometallics* **2001**, *20*, 2417−2420. (i) Kaul, F. A. R.; Puchta, G. T.; Schneider, H.; Grosche, M.; Mihalios, D.; Herrmann, W. A. *J. Organometallic Chem.* **2001**, *621*, 177−183. (j) Chen, Y.-X.; Kruper, W. J.; Roof G.; Wilson, D. R. *J. Am. Chem. Soc.* **2001**, *123*, 745−746. (k) Zhou, J.; Lancaster, S. J.; Walker, D. A.; Beck, S.; Thornton-Pett, M.; Bochmann, M. *J. Am. Chem. Soc.* **2001**, *123*, 223−237. (l) Kehr, G.; Roesmann, R.; Frohlich, R.; Holst, C.; Erker, G. *Eur. I. Inorg. Chem.* **2001**, 535−538. (m) Mager, M.; Becke, S.; Windisch, H.; Denninger, U. *Angew. Chem., Int. Ed. Engl.* **2001**, *40*, 1898−1902. (n) Chase, P. A.; Piers, W. E.; Patrick, B. O.; *J. Am. Chem. Soc.* **2000**, *122*, 12 911−12 912. (o) LaPointe, R. E.; Roof, G. R.; Abboud, K. A.; Klosin, J. *J. Am. Chem. Soc.* **2000**, *122*, 9560−9561. (p) Sun, Y. M.; Metz, M. V.; Stern, C. L.; Marks, T. J. *Organometallics* **2000**, *19*, 1625−1627. (q) Metz, M. V.; Schwartz, D. J.; Stern, C. L.; Nickias, P. N.; Marks, T. J. *Angew. Chem., Int. Ed. Engl.* **2000**, *39*, 1312−1316.

(3) (a) Sinn, H.; Kaminsky, W. *Adv. Organomet. Chem.* **1980**, *18*, 99−149. (b) Sinn, H.; Kaminsky, W.; Vollmer, H.-J.; Woldt, R. *Angew. Chem., Int. Ed. Engl.* **1980**, *19*, 390−392.

(4) (a) Yang, X.; Stern, C. L.; Marks, T. J. *J. Am. Chem. Soc.* **1994**, *116*, 10 015−10 031. (b)Yang, X.; Stern, C. L.; Marks, T. J. *J. Am. Chem. Soc.* **1991**, *113*, 3623−3625. (c) Ewen, J. A.; Elder, M. J. *Chem. Abstr.* **1991**, *115*, 136 998g.

(5) (a) Li, L.; Stern, C. L.; Marks, T. J. *Organometallics* **2000**, *19*, 3332−3337. (b) Li, L.; Marks, T. J. *Organometallics* **1998**, *17*, 3996−4003. (c) Chen, Y.-X.; Stern, C. L.; Yang, S.; Marks, T. J. *J. Am. Chem. Soc.* **1996**, *118*, 12 451−12 452.6. (d) also see ref 2c,d. (e) For a recent chelating borane review, see: Piers, W. E.; Irvine, G. J.; Williams, V. C. *Eur. J. Inorg. Chem.* **2000**, 2131−2142.

(6) (a) Chien, J. C. W.; Tsai, W.-M.; Rausch, M. D. *J. Am. Chem. Soc.* **1991**, *113*, 8570−8571. (b) Yang, X.; Stern, C. L.; Marks, T. J. *Organometallics* **1991**, *10*, 840−842. (c) Ewen, J. A.; Elder, M. J. *Eur. Pat. Appl.* 426637 **1991**; *Chem. Abstr.* **1991**, *115*, 136 987c, 136 988d.

(7) For related fluorinated tetraarylborates, see: (a) Kaul, F. A. R.; Puchta, G. T.; Schneider, H.; Grosche, M.; Mihalios, D.; Herrmann, W. A. *J. Organomet. Chem.* **2001**, *621*, 184−189. (b) also see refs 2g,h,k. (c) Jia, L.; Yang, X.; Stern, C. L.; Marks, T. J. *Organometallics* **1997**, *16*, 842−857. (d) Jia, L.; Yang, X.; Ishihara, A.; Marks, T. J. *Organometallics* **1995**, *14*, 3135−3137.

(8) (a) Chen, Y.-X.; Metz, M. V.; Li, L.; Stern, C. L.; Marks, T. J. *J. Am. Chem. Soc.* **1998**, *120*, 6287−6305. (b) Chen, Y. X.; Stern, C. L.; Marks, T. J. *J. Am. Chem. Soc.* **1997**, *119*, 2582−2583. (c) Elder, M. J.; Ewen, J. A. *Eur. Pat. Appl. EP* 573, 403, 1993; *Chem. Abstr.* **1994**, *121*, 0207d. (d) also see Ref. 2o.

(9) (a) Razavi, A.; Thewalt, U. *J. Organomet. Chem.* **1993**, *445*, 111−114. (b) Razavi, A.; Ferrara, J. *J. Organomet. Chem.* **1992**, *435*, 299−310.

(10) Chen, M.-C.; Marks, T. J. *J. Am. Chem. Soc.* **2001**, *123*, 11 803−11 804.

(11) (a) Resconi, L.; Cavallo, L.; Fait, A.; Piemontesi, F. in ref. 1c, pp 1253−1345. (b) Coates, G. W. in ref 1c, pp 1223−1252. (c) Veghini, D.; Henling, L. M.; Burkhardt, T. J.; Bercaw, J. E. *J. Am. Chem. Soc.* **1999**, *121*, 564−573. (d) Ewen, J. A.; Jones, R. L.; Razavi, A.; Ferrara, J. D. *J. Am. Chem. Soc.* **1988**, *110*, 6255−6256.

(12) (a) Beswick, C. L.; Marks, T. J. *J. Am. Chem. Soc.* **2000**, *122*, 10 358−10 370. (b) Deck, P. A.; Beswick, C. L.; Marks, T. J. *J. Am. Chem. Soc.* **1998**, *120*, 1772−1784. (c) Luo, L.; Marks, T. J. in ref 1d, pp 97−106. (d) also see refs 7c and 8a.

(13) (a) See ref 2a. (b) Busico, V.; Cipullo, R. *Prog. Polym. Sci.* **2001**, *26*, 443−533. (c) Farina, M.; Terragni, A. *Makromol. Chem., Rapid Commun.* **1993**, *14*, 791−798. (d) Such techniques are reviewed in ref 11a.

Scheme 1

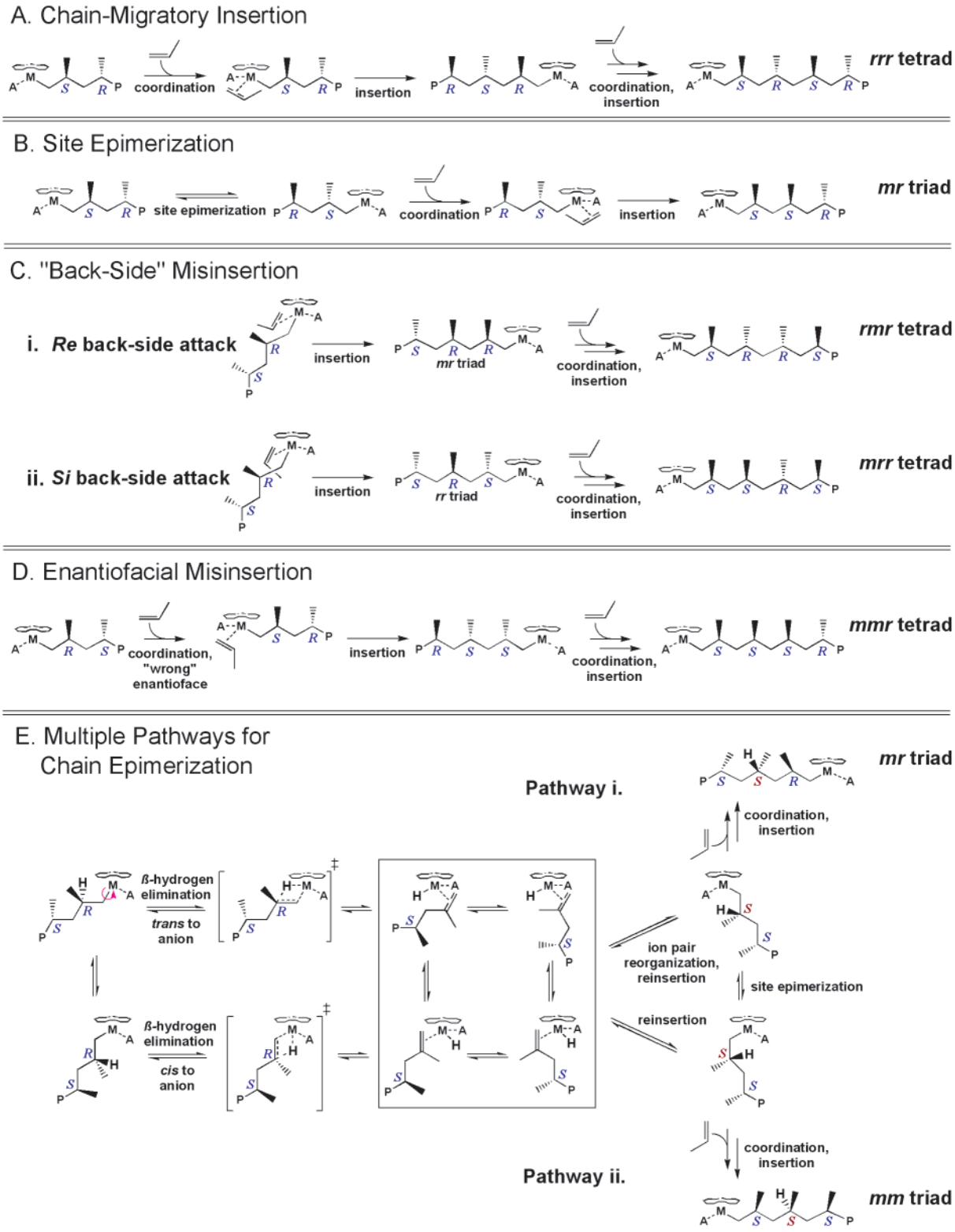

$MeB(C_6F_5)_3^-$ systems and their sensitivity to Li^+ $MeB(C_6F_5)_3^-$ addition[14] prompt questions about potential ion pair aggregation effects on enchainment in this system. Thus, catalyst concentration effects are also examined here, as are possible influences of counteranion exchange and added Li^+ $MeB(C_6F_5)_3^-$ on propylene polymerization. To further detail and elucidate solvent polarity effects on ion pairing during polymerization, cocatalyst effects in an even less polar solvent, octane, are compared to previous results. In addition, the spectrum of cocatalysts studied has been expanded to include MAO, to compare ion-pairing effects in this broadly utilized cocatalyst to the previously investigated species. Propylene polymerization catalyzed by **1**+MAO is carried out over a range of temperatures and propylene pressures, and in the various solvents, and these

(14) Beck, S.; Lieber, S.; Schaper, F.; Geyer, A.; Brintzinger, H. H. J. *J. Am. Chem. Soc.* **2001**, *123*, 1483−1489.

results are compared to those obtained with the other cocatalysts. In addition, X-ray crystallographic characterization of $[Me_2C(Cp)(Flu)]ZrMe^+$ $MeB(C_6F_5)_3^-$ (**7**) and $[Me_2C(Cp)(Flu)]ZrMe^+$ $FAl(2\text{-}C_6F_5C_6F_4)_3^-$ (**10**), and determination of the solution phase molecular dynamics of these complexes, lead to a description of the molecular basis for catalytic activity and selectivity. Compared to $B(C_6F_5)_4^-$, $CH_3B(C_6F_5)_3^-$, which is commonly accepted as more strongly coordinating, exhibits an expected lower polymerization activity,[1b,7c,7d] but surprisingly and without precedent, *lower* polypropylene stereoregularity. Using a straightforward kinetic model, we provide here a rationalization of this interesting, counterintuitive result and then generalize it to all of the cocatalyst systems examined here.

Experimental Section

Materials and Methods. All manipulations of air-sensitive materials were performed with rigorous exclusion of oxygen and moisture in flamed Schlenk-type glassware on a dual-manifold Schlenk line or interfaced to a high-vacuum line (10^{-6} Torr), or in an N_2-filled Vacuum Atmospheres glovebox with a high capacity recirculator (<1 ppm O_2). Argon (Matheson, prepurified), and propylene (Matheson, polymerization grade) were purified by passage through a supported MnO oxygen-removal column and an activated Davison 4A molecular sieve column. Hydrocarbon solvents (toluene and pentane) were distilled under nitrogen from Na/K alloy/benzophenone ketyl. All solvents for high-vacuum line manipulations were stored in vacuo over Na/K alloy in Teflon-valved bulbs. Deuterated solvents were obtained from Cambridge Isotope Laboratories (all ≥ 99 atom %D), were freeze−pump−thaw degassed, dried over Na/K alloy, and stored in re-sealable flasks. Other nonhalogenated solvents were dried over Na/K alloy, and halogenated solvents were distilled from CaH_2. Methylaluminoxane (MAO, obtained as a toluene solution from Aldrich) was dried under high vacuum for 24 h to remove excess volatile aluminum alkyls before use. $[Me_2C(Cp)(Flu)]ZrMe_2$ (**1**),[9] $B(C_6F_5)_3$ (**3**),[15] $B(2\text{-}C_6F_5C_6F_4)_3$ (**4**),[8a] $Ph_3C^+B(C_6F_5)_4^-$ (**5**),[6] $Ph_3C^+FAl(2\text{-}C_6F_5C_6F_4)_3^-$ (**6**)[8a] were prepared according to literature procedures.

Physical and Analytical Measurements. NMR spectra were recorded on Varian ^{UNITY}Inova-500 (FT, 500 MHz, ^{1}H; 125 MHz, ^{13}C), ^{UNITY}Inova-400 (FT, 400 MHz, ^{1}H; 100 MHz, ^{13}C), Mercury-400 (FT 400 MHz, ^{1}H; 100 MHz, ^{13}C; 377 MHz, ^{19}F) or Gemini-300 (FT 300 MHz, ^{1}H; 75 MHz, ^{13}C; 282 MHz, ^{19}F) instruments. Variable-temperature measurements were carried out using the ^{UNITY}Inova-400 instrument with a 5-mm inverse probe or 5-mm broadband probe. Probehead temperature calibration was conducted using methanol and ethylene glycol standard samples (Varian, Inc.). Chemical shifts for ^{1}H and ^{13}C spectra were referenced using internal solvent resonances and are reported relative to tetramethylsilane. ^{19}F NMR spectra were referenced to external $CFCl_3$. NMR experiments on air-sensitive samples were conducted in Teflon valve-sealed NMR tubes (J. Young). For ^{13}C NMR analyses of homopolymer microstructures, 300∼400 mg polymer samples were dissolved in 4 mL $C_2D_2Cl_4$, heated with a heat gun in a 10 mm NMR tube, and transferred to the NMR spectrometer with the probehead pre-equilibrated at 125 °C. A 2.0 s acquisition time was used with a pulse delay of 6.0 s. A total of 4000−6000 transients were accumulated for each spectrum. Pentad signals were assigned according to literature criteria.[16] Melting temperatures of polymers were measured by DSC (DSC 2920, TA Instruments, Inc.) from the second scan with a heating rate of 10 °C/min. GPC analyses of polymer samples were performed at the Dow Chemical Co., Chemical Sciences Catalysis Laboratory, Midland, Michigan, on a Waters Alliance GPCV 2000 high-temperature instrument. A polystyrene/polypropylene universal calibration was carried out using polystyrene standards.

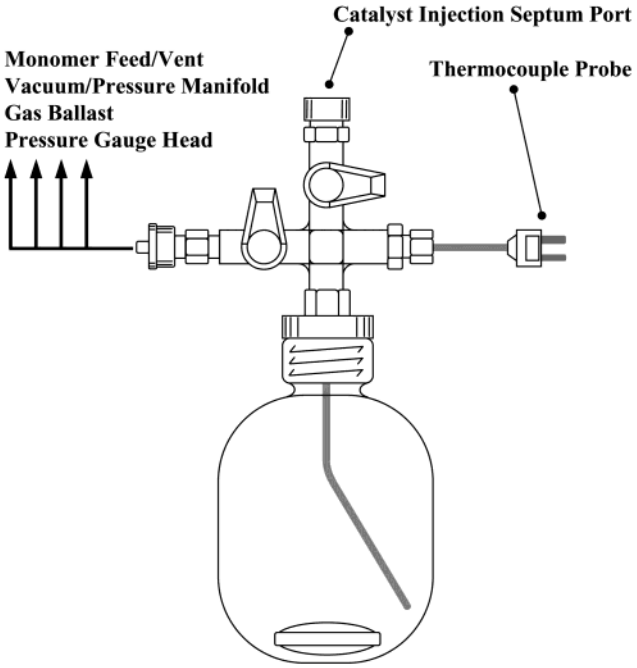

Figure 1. High-pressure polymerization reaction system.

Propylene Polymerization Experiments. Ambient-pressure propylene polymerizations were carried out on a high vacuum line (10^{-6} Torr) in 250 mL round-bottom three-neck Morton flasks equipped with large magnetic stirring bars, and with rapid stirring (∼1000 rpm) to minimize mass transfer,[17] and thermocouple probes to monitor exotherm effects.[2c] In a typical experiment, dry toluene (50 mL) was vacuum transferred into the flask from Na/K, presaturated under 1.0 atm of rigorously purified propylene, and equilibrated at the desired reaction temperature using an external water bath. The catalytically active species was freshly generated in 2∼4 mL of dry toluene in the glovebox. Control NMR experiments revealed quantitative activation of the catalyst under these conditions (vide infra). The catalyst solution was then quickly injected into the rapidly stirred flask using a gastight syringe. The temperature of the reaction mixture during polymerization was monitored in real time using a thermocouple thermometer (OMEGA Type K). The temperature rise was invariably less than 3 °C during these polymerizations, and temperature was controlled by occasional addition of ice to the external water bath. After a measured time interval, the reaction was quenched by the addition of 10 mL 2% acidified methanol. Another 300−400 mL methanol was then added and the polymer was collected by filtration, washed with methanol, and dried on the high vacuum line to a constant weight.

High-pressure polymerization experiments in toluene solutions were carried out in a 350 mL heavy wall glass pressure reactor, (Chemglass Co., maximum pressure, 10 atm) equipped with a septum port, a large magnetic stirring bar (∼1000 rpm), and an internal thermocouple (OMEGA Type K), and connected to a high-pressure manifold equipped with a gas inlet, diaphragm capacitance pressure gauge (0−200 psig), and gas outlet (Figure 1). **CAUTION: All of these procedures should be performed behind a blast shield.** In a typical procedure, in glovebox, the reactor was charged with dry toluene (50 mL) and the apparatus was assembled, removed, and then connected to the high-pressure manifold. Under rapid stirring, rigorously purified propylene was pressurized into the flask to reach ∼5−6 atm over 5 min and then

(15) Massey, A. G.; Park, A. J. *J. Organomet. Chem.* **1964**, *2*, 245−250.
(16) (a) Busico, V.; Cipullo, R.; Monaco, G.; Vacatello, M. *Macromolecules* **1997**, *30*, 6251−6263. (b) Pellecchia, C.; Pappalardo, D.; D′Arco, M.; Zambelli, A. *Macromolecules* **1996**, *29*, 1158. (c) Busico, V.; Cipullo, R.; Corradini, P.; Landriani, L.; Vacatello, M.; Segre, A. L. *Macromolecules* **1995**, *28*, 1887. (d) Miyatake, T.; Miaunuma, K.; Kakugo, M. *Macromol. Symp.* **1993**, *66*, 203. (e) Kakugo, M.; Miyatake, T.; Miaunuma, K. *Stud. Surf. Sci. Catal.* **1990**, *56*, 517. (f) Longo, P.; Grassi, A. *Makromol. Chem.* **1990**, *191*, 2387. (g) Randall, J. C. *J. Polym. Sci., Part B: Polym. Phys.* **1975**, *13*, 889.

slowly released to 1.0 atm over 5 min. This fill and release process was repeated five times. The solution was then equilibrated at the desired propylene pressure (1.0−5.0 atm) and reaction temperature adjusted using an external water bath. Preparation of the catalytically active species, temperature control, and reaction quenching were performed as described for ambient-pressure reactions. Propylene pressure was then released to 1.0 atm and polypropylene workup was carried out using the procedure described above. Polymerization experiments in 1,3-dichlorobenzene or octane solutions were carried out as described above, but with addition of 50 mL dry 1,3-dichlorobenzene or octane by cannula through the septum port. Ion pair complexes were prepared and introduced as described above.

Microstructural Analysis of Polypropylene ^{13}C NMR Spectra. Polymer methyl resonances were assigned according to established criteria,[16] and were analyzed at the pentad level. All polymer NMR spectra were collected with identical temperature, solvent, instrument field strength, and acquisition and processing parameters. Steric pentad distributions were determined from direct integration of the following regions (ppm): δ 21.91−21.7 (*mmmm*); 21.63−21.46 (*mmmr*); 21.43−21.24 (*rmmr*); 21.16−20.94 (*mmrr*); 20.94−20.74 (x*rm*x); 20.74−20.58 (*rmrm*); 20.58−19.74 (*rrrr* + *rrrm* + *mrrm*). Pentad distributions were modeled using the syndiospecific Bernoullian model outlined in Table 16 of ref 11a (p. 1316), having probability parameters P_m and P_{mm} of formation for *m* and *mm* stereodefects, respectively. These probabilities were determined by successive nonlinear least-squares minimization of the function

$$wR^2 = \frac{\sum (I_{exp} - I_{calcd})^2 (1 + I_{exp})^w}{\sum {I_{exp}}^2} \qquad (3)$$

where I_{exp} and I_{calcd} are experimental and calculated integral values (normalized to $\Sigma I_{exp} = 1$) with weighting factor $w = 25$ for all regions, with the exception of the *rrrr* + *rrrm* + *mrrm* integral, for which $w = 0$. This weighting scheme increases the contribution to wR^2 of stronger signals (having greater S/N ratios), while ensuring that the *rrrr* + *rrrm* + *mrrm* integral, which is substantially larger than the rest, does not dominate the refinement. Agreement factors calculated according to the standard method, $R^2 = \Sigma(I_{exp} - I_{calcd})^2/\Sigma(I_{exp})^{2,13c}$ are less than 0.001 in all but two cases, with 0.0022 the highest value. I_{exp}, I_{calcd}, and weighting multipliers $(1 + I_{exp})^w$, for each experiment, along with P_m, P_{mm}, wR^2, and R^2 for each set, are given in the Supporting Information.

Reaction of [Me$_2$C(Cp)(Flu)]ZrMe$_2$ with B(C$_6$F$_5$)$_3$, B(2-C$_6$F$_5$C$_6$F$_4$)$_3$, Ph$_3$C$^+$B(C$_6$F$_5$)$_4^-$, or Ph$_3$C$^+$ FAl(2-C$_6$F$_5$C$_6$F$_4$)$_3^-$. [Me$_2$C(Cp)(Flu)]-ZrMe$_2$ (**1**) and cocatalysts (**3**−**6**) were loaded into a J. Young NMR tube and 0.5 mL of toluene-d_8 was transferred in via pipet. Each sample was then shaken vigorously and removed directly to the NMR spectrometer. Reagents **1** (3.9 mg, 10 μmol) and **3** (B(C$_6$F$_5$)$_3$, 5.1 mg, 10 μmol) were combined, and complete reaction with rapid formation of [Me$_2$C(Cp)(Flu)]ZrMe$^+$MeB(C$_6$F$_5$)$_3^-$ (**7**) was observed (NMR data are presented below). Reagents **1** (3.9 mg, 10 μmol) and **4** (B(2-C$_6$F$_5$C$_6$F$_4$)$_3$, 4.8 mg, 5.0 μmol) were combined, and complete reaction with rapid formation of {([Me$_2$C(Cp)(Flu)]ZrMe)$_2$(μ-Me)}$^+$ MeB(2-C$_6$F$_5$C$_6$F$_4$)$_3^-$ (**8**) was observed. ^{1}H and ^{19}F NMR data for **8** are given in a previous report.[8a] Reagents **1** (1.0 mg, 2.5 μmol) and **5** (Ph$_3$C$^+$B(C$_6$F$_5$)$_4^-$, 2.3 mg, 2.5 μmol) were combined, and complete reaction with rapid formation of [Me$_2$C(Cp)(Flu)]ZrMe$^+$ B(C$_6$F$_5$)$_4^-$ (**9**) and Ph$_3$CCH$_3$ was observed. The C$_6$H$_4$ signals of the fluorenyl region could not be assigned completely due to overlap of the signals with the solvent. ^{1}H NMR for **9** (C$_7$D$_8$, 23 °C): δ 7.8 (d, 1 H, C$_6$H$_4$), 7.6 (d, 1 H, C$_6$H$_4$), 5.742 (m, 1 H, C$_5$H$_4$), 4.824 (m, 1 H, C$_5$H$_4$), 4.435 (m, 1 H,C$_5$H$_4$), 3.813 (m, 1 H, C$_5$H$_4$), 1.667 (s, 3 H, CMe$_2$), 1.477 (s, 3 H, CMe$_2$), −1.142 (s, 3 H, Zr−CH$_3$). ^{19}F NMR (C$_7$D$_8$, 23 °C): δ −132.06 (m, *o*-F), −132.49 (m, *o*-F), −162.77 (t, $^3J_{F-F}$ = 21.5 Hz, *p*-F), −163.0 (m, *p*-F), −166.72 (m, *m*-F), −166.96 (m, *m*-F). Prolonged standing of complex **9** results in a red-brown oily residue, and the solution gradually turns brown-green. In a reaction of **1** with **5** at a 4-fold higher concentration, the red-brown oily residue forms immediately, and generates mixtures of unidentified complexes. Reagents **1** (2.0 mg, 0.005 mmol) and **6** (Ph$_3$C$^+$FAl(2-C$_6$F$_5$C$_6$F$_4$)$_3^-$, 6.5 mg, 0.0050 mmol) were combined and complete reaction of **1** with rapid formation of [Me$_2$C-(Cp)(Flu)]ZrMe$^+$ FAl(2-C$_6$F$_5$C$_6$F$_4$)$_3^-$ (**10**) and Ph$_3$CCH$_3$ was observed (NMR data are presented below).

In Situ Generation of Ion Pairs 7−10 for Polymerization Studies. [Me$_2$C(Cp)(Flu)]ZrMe$_2$ (**1**) and the required cocatalyst in a 1:1 ratio (**3**, **5**, **6**) or a 0.5:1 ratio (**4**) were loaded in the glovebox into a vial equipped with a septum, and 2−4 mL of toluene was added. The mixture was shaken vigorously at room temperature for 10 min (**3**, **4**, **6**) or 2 min (**5**) before use. Total amounts used were chosen/refined as required for temperature control and are reported herein (see Tables 7, 8, and 12−14).

Synthesis of [Me$_2$C(Cp)(Flu)]ZrMe$^+$ MeB(C$_6$F$_5$)$_3^-$ (7). In the glovebox, [Me$_2$C(Cp)(Flu)]ZrMe$_2$ (**1**, 97.5 mg, 0.250 mmol), B(C$_6$F$_5$)$_3$ (**3**, 128 mg, 0.250 mmol), and 50 mL toluene were loaded into a 100-mL reaction flask having a filter frit and stirred for 2 h at room temperature. The solvent was next reduced in vacuo to 10 mL, and 50 mL pentane was condensed into the flask. The resulting suspension was filtered, and the collected solid was washed with 5 mL of pentane and dried under vacuum to afford 174 mg of the title complex; yield, 77%. ^{1}H NMR peak assignments are determined from combined 1-D and 2-D NMR techniques, and are as follows (labeling outlined in **C**): ^{1}H NMR (C$_7$D$_8$, 23 °C): δ 7.65 (d, J_{H-H} = 8.5 Hz, 1 H, H$_A$), 7.60 (d, J_{H-H} = 8.5 Hz, 1 H, H$_{A'}$), 7.12 (d, J_{H-H} = 6.3 Hz, 1 H, H$_B$), 7.05 (d, J_{H-H} = 8.2 Hz, 1 H, H$_D$), 6.92 (d, J_{H-H} = 8.3 Hz, 1 H, H$_{D'}$), 6.74 (t, J_{H-H} = 7.7 Hz, 1 H, H$_C$), 6.63 (t, J_{H-H} = 7.1 Hz, 1 H, H$_{C'}$), 6.41 (t, J_{H-H} = 8.2 Hz, 1 H, H$_{B'}$), 5.93 (d, J_{H-H} = 3.0 Hz, 1 H, H$_{F'}$), 5.55 (d, J_{H-H} = 3.0 Hz, 1 H, H$_F$), 5.20 (d, J_{H-H} = 3.0 Hz, 1 H, H$_E$), 4.45 (d, J_{H-H} = 3.0 Hz, 1 H, H$_{E'}$), 1.50 (s, 3 H, Me$_R$), 1.46 (s, 3 H, Me$_{R'}$), −0.53 (s, br, 3 H, Me$_B$), −0.92 (s, 3 H, Me$_M$). ^{19}F NMR (C$_7$D$_8$, 23 °C): δ −133.39 (d, $^3J_{F-F}$ = 22.60 Hz, 6 F, *o*-F), −159.60 (t, $^3J_{F-F}$ = 20.6 Hz, 3 F, *p*-F), −164.62 (t, $^3J_{F-F}$ = 18.3 Hz, 6 F, *m*-F). Anal. Calcd. for C$_{41}$H$_{24}$BF$_{15}$Zr: C, 54.49; H, 2.68. Found: C, 54.37; H, 2.84.

C

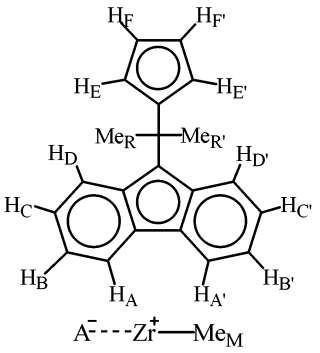

A$^-$ = Me$_B$B(C$_6$F$_5$)$_3^-$, **7**; A$^-$ = FAl(C$_{12}$F$_9$)$_3^-$, **10**

Synthesis of [Me$_2$C(Cp)(Flu)]ZrMe$^+$ FAl(2-C$_6$F$_5$C$_6$F$_4$)$_3^-$ (10). In the glovebox, [Me$_2$C(Cp)(Flu)]ZrMe$_2$ (**1**, 97.5 mg, 0.250 mmol), Ph$_3$C$^+$-FAl(2-C$_6$F$_5$C$_6$F$_4$)$_3^-$ (**6**, 328 mg, 0.250 mmol), and 100 mL toluene were loaded into a 250 mL reaction flask having a filter frit, and stirred for 2 h at room temperature. The solvent was next reduced in vacuo to 10 mL, and 100 mL pentane was condensed into the flask. The resulting suspension was filtered, and the collected solid was washed with 20 mL of pentane and dried under vacuum to afford 280 mg of the title complex; yield, 82%. As measured from ^{1}H spectra, a pair of diastereomers is evident in a 1.6:1 ratio at 23 °C. Assignment of the ^{1}H NMR spectrum was accomplished with combined NOE, EXSY, and COSY techniques; atom labeling is described in **C**. Major and minor

diastereomers are differentiated with upper- and lower-case subscripts, respectively. Certain of the C_6H_4 signals of the fluorenyl region could not be clearly assigned due to overlap between the signals of the two isomers. ^{1}H NMR (C_7D_8, 23 °C) for major diastereomer: δ 7.99 (d, J_{H-H} = 8.0 Hz, 1 H, $H_{A'}$), 7.90 (dm, J_{H-H} = 4.0 Hz, 1 H, H_A), 7.20 (m, 2 H, $H_{B'}$ and H_D), 7.00 (1 H, $H_{D'}$), 6.78 (m, 2 H, H_C and $H_{C'}$), 6.20 (s, 1 H, $H_{F'}$), 6.08 (t, J_{H-H} = 8.0 Hz, 1 H, H_B), 5.44 (m, 1 H, H_E), 4.85 (s, 1 H, H_F), 4.61 (m, 1 H, $H_{E'}$), 1.61 (s, 3 H, Me_R), 1.44 (s, 3 H, $Me_{R'}$), −1.03 (s, 3 H, Me_M). Minor diastereomer: δ 7.65 (d, J_{H-H} = 8.4 Hz, 1 H, $H_{a'}$), 7.55 (dm, J_{H-H} = 8.0 Hz, 1 H, H_a), 7.20 (m, 1 H, H_d), 7.09 (1 H, $H_{b'}$), 7.00 (2 H, H_c and $H_{d'}$), 6.74 (m, 1 H, $H_{c'}$), 6.32 (s, 1 H, Hf'), 5.99 (t, J_{H-H} = 8.0 Hz, 1 H, H_b), 5.44 (m, 1 H, H_e), 5.00 (s, 1 H, H_f), 4.58 (m, 1 H, $H_{e'}$), 1.65 (s, 3 H, Me_r), 1.50 (s, 3 H, $Me_{r'}$), −1.07 (s, 3 H, Me_m). ^{19}F NMR (C_7D_8, 23 °C) for major diastereomer: δ −113.62 (s, br, 3F), −133.90 (m, 3F), −134.60 (s, br, Al−F), −138.04 (m, 3F), −139.24 (t, $^3J_{F-F}$ = 21.5 Hz, 3F), 153.27 (t, $^3J_{F-F}$ = 19.8 Hz, 6F), 154.87 (m, 3F), 161.38 (m, 3F), 163.03 (t, $^3J_{F-F}$ = 21.2 Hz, 3F). Minor diastereomer: δ 116.01 (s, br, 3F), −132.42 (s, br, Al−F), −133.90 (m, 3F), −138.68 (m, 3F), −139.55 (t, $^3J_{F-F}$ = 18.9 Hz, 3F), 153.52 (t, $^3J_{F-F}$ = 21.2 Hz, 3F), 153.68 (t, $^3J_{F-F}$ = 23.7 Hz, 3F), 153.89 (m, 3F), 161.22 (dd, J_{F-F} = 21.2, 7.6 Hz, 3F), 162.84 (t, $^3J_{F-F}$ = 23.7 Hz, 3F). Anal. Calcd for $C_{58}H_{21}AlF_{28}Zr$: C, 50.92; H, 1.55. Found: C, 50.64; H, 1.73.

X-ray Crystal Structure Determinations of [Me_2C(Cp)(Flu)]ZrMe$^+$ MeB(C_6F_5)$_3^-$ (7) and [Me_2C(Cp)(Flu)]ZrMe$^+$ FAl(2-$C_6F_5C_6F_4$)$_3^-$ (10). Crystals of the title complexes suitable for X-ray diffraction were obtained by slow diffusion of pentane into toluene solutions at 0 °C. Crystals were selected and mounted under Infineum V8512 oil, and held under a nitrogen cold-stream at 153(2) K for data collection. Diffraction data were obtained using a Bruker SMART 1000 CCD area detector diffractometer with a fine-focus, sealed tube Mo Kα radiation source (λ = 0.71073 Å) and graphite monochromator. For both 7 and 10, the initial crystal structure solution was obtained via Patterson synthesis, refined through successive least-squares cycles, and subjected to a face-indexed absorption correction. The refinements were carried to convergence, with hydrogen atoms placed in idealized positions and refined isotropically with fixed U_{eq} under standard riding model constraints, with the following exception: in complex 7, hydrogen atoms H_3C−B were refined isotropically with group thermal, H−C distance, and H−H distance parameters. Crystal data collection and refinement parameters are summarized in Table 1 and can be found in the Crystallographic Information File (CIF, see Supporting Information).

2D EXSY NMR Studies of Ion Pair Reorganization/Symmetrization in 7 and 10. Toluene-d_8 solutions of pure [Me_2C(Cp)(Flu)]ZrMe$^+$ MeB(C_6F_5)$_3^-$ (**7**, 4.0 mg, 5.5 μM) or [Me_2C(Cp)(Flu)]ZrMe$^+$ FAl(2-$C_6F_5C_6F_4$)$_3^-$ (**10**, 7.0 mg, 6.4 μM) were prepared in the glovebox, and filtered directly into J. Young NMR tubes. Spectra were collected using the NOESY pulse sequence,[18] with acquisition parameters optimized to resolve peaks of interest. Mixing times τ_m = 40−800 ms, were chosen to minimize the error in calculated exchange rates, according to $\tau_m = (T_1^{-1} + k_{AB} + k_{BA})^{-1}$, where k_{AB} and k_{BA} are estimates of the A→B and B→A exchange rate constants, respectively.[19] Data were zero-filled to 2 × np and 4 × ni in the t_2 and t_1 dimensions, respectively, and apodized using appropriate Gaussian weighting in the t_2 dimension and combined Gaussian weighting and 1 Hz line-broadening in the t_1 dimension, unless otherwise noted. Rate constant calculations are described in the discussion.[19] For **7** (τ_m = 600 ms, 20.5 °C), quadrupolar relaxation of the ^{11}B- and ^{10}B-coupled Me_B protons precludes accurate determination of rates for exchange involving these resonances using this technique. For **10**, exchange rates between resonances H_A and H_a and between $H_{A'}$ and $H_{a'}$ were averaged to determine anion racemization rates at 87.5 °C (τ_m = 185 ms) and 117.5 °C (τ_m = 40 ms). Anion racemization rate constants calculated from EXSY data are in good agreement with values obtained from line shape analysis (vide infra). At 127 °C, τ_m was optimized to determine, or to place a higher limit on, the rate of ion pair reorganization (τ_m = 800ms). In this case, 14 000 real points in the t_2 dimension and 256 points in the t_1 dimension were collected, and the data were processed with no zero-filling and 1 Hz line broadening in t_2, and with linear prediction to 512 points, zero-filling to 8192 points, 1 Hz line broadening, and 0.036 s Gaussian weighting in t_1. With **10**, cross-peaks corresponding to ion pair reorganization are absent at all temperatures measured, invariantly with mixing time and data processing parameters. An upper limit for ion pair reorganization is established as described in the Discussion Section.

DNMR Studies of Ion Pair Reorganization/Symmetrization in 7 and 10 in Toluene-d_8. Pure [Me_2C(Cp)(Flu)]ZrMe$^+$ MeB(C_6F_5)$_3^-$ (**7**, 8.0 mg, 8.8 μmol) or [Me_2C(Cp)(Flu)]ZrMe$^+$ FAl(2-$C_6F_5C_6F_4$)$_3^-$ (**10**, 7.0 mg, 5.1 μmol) were loaded in the glovebox into capped vials, and 0.80 mL of a stock solution of $CH_3Si(C_6H_5)_3$ (internal standard, 11 mM for **7** and 6.4 mM for **10**) in toluene-d_8 was transferred into each vial. The resultant solutions were filtered and transferred into J. Young NMR tubes. Temperatures were varied over the range 0−92.5 °C for **7**, and over 23−132.5 °C for **10**. Prior to each acquisition, the NMR probehead was preequilibrated at the desired temperature for 10 min. Each acquisition consisted of 65536 points spanning 4360 Hz (resolution 0.067 Hz), and 4908 Hz (resolution 0.075 Hz), for **7** and **10**, respectively. The raw data were zero-filled to 2 × np. Unweighted transforms for both **7** and **10** were phased carefully and subjected to reference deconvolution on the methyl resonance of triphenylmethylsilane as the internal line shape standard using the Hilbert algorithm,[20]

Table 1. Summary of the Crystal Structure Data for Complexes **7** and **10**[a]

complex	**7**	**10**
formula	$C_{48}H_{32}BF_{15}Zr$	$C_{58}H_{21}Al\,F_{28}Zr$
formula weight	995.77	1367.95
crystal color, habit	red, plate	red, block
crystal dimensions (mm)	0.284 × 0.178 × 0.044	0.194 × 0.174 × 0.166
crystal system	monoclinic	monoclinic
space group	$P2_1/c$	$P2_1/c$
a, Å	13.5302 (18)	16.4939 (10)
b, Å	26.815 (4)	19.6187 (12)
c, Å	12.4684 (16)	16.9722 (10)
β, deg	116.673 (2)	112.4710 (10)
V, Å^3	4042.3 (9)	5075.0 (5)
Z	4	4
d (calc), g/cm^3	1.636	1.790
μ, mm^{-1}	0.378	0.380
$T_{min}-T_{max}$	0.91577−0.98342	0.925 39−0.952 86
measured reflections	35 835	46 570
independent reflections	9692	12346
reflections > 2σ (I)	4357	8033
R_{int}	0.1409	0.0705
$R[F^2 > 2\sigma(F^2)]$	0.0548	0.0503
$wR(F^2)$	0.1344	0.1374
S	0.880	0.981
no. of parameters	601	796

[a] CCD area detector diffractometer; φ and ω scans; temperature for data collection, 153 (2) K; Mo Kα radiation; λ = 0.710 73 Å.

(17) At 20 °C, rate of C_3H_6 absorption is estimated 0.029 mol/min in toluene at 1.0 atm of C_3H_6, and propylene mass transfer effects (mass transport coefficient) in the (2-PhInd)$_2ZrCl_2$/ MAO system in toluene (100 mL) are observed to be insensitive to the presence of up to 4 g of isotactic PP with a maximum stirring speed (1460 rpm), See: Lin, S.; Tagge, C. D.; Waymouth, R. M.; Nele, M.; Collins, S.; Pinto, J. C. *J. Am. Chem. Soc.* **2000**, *122*, 11 275−11 285. In the present study, the most active ion pair system, **5** (**9**) at 40 °C and 1.0 atm of C_3H_6, has a maximum rate of propylene consumption of ∼0.015 mol/min (0.77/42*(75/60)), which should be lower at 20 °C because lower activity is observed at lower temperatures. Thus, propylene mass transfer effects should be negligible for all catalysts under the present conditions.

(18) Macura, S.; Ernst, R. R. *Mol. Phys.* **1980**, *41*, 95−117.

(19) Perrin, C. L.; Dwyer, T. J. *Chem. Rev.* **1990**. *90*, 935−967, and also see ref 14.

(20) Rutledge, D. N., Ed. *Signal Treatment and Signal Analysis in NMR;* Elsevier Science: New York, 2003; Ch. 16.

Scheme 2. X⁻, X′⁻ represent alternate stereochemical configurations at Al[a]

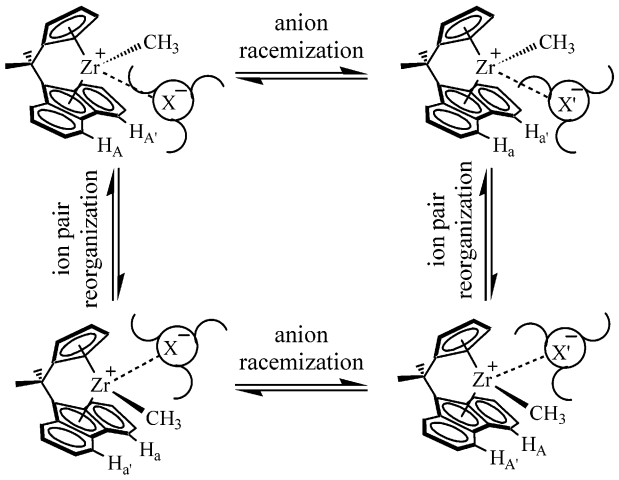

10, X^-, $X'^- = FAl(2\text{-}C_{12}F_9)_3^-$

[a] The symbols used to represent these configurations are intended to convey a qualitative picture of anion racemization (see Figure 4).

along with baseline and drift corrections, such that the final standard peak width was 1.500 Hz in all spectra. Modeling of the ^{29}Si satellites of the reference signal was included in the reference deconvolution ($^2J_{Si-H} = 6.633$ Hz). Application of reference deconvolution was found to significantly improve variances, both for borane migration and for ion pair reorganization, compared to line fits generated from use of the approximation for half-height signal widths, $W_{signal} = W_{real} + \Delta W_{natural} + \Delta W_{exchange}$. For **7**, broadening of the proton signals of the diastereotopic *i*-Pr methyl groups (Me_R, $Me_{R'}$) and of the zirconocenium methyl group (Me_M) were monitored over the temperature range, 57.8−92.3 °C. Rate constants at each temperature were calculated from the half-height widths of these signals (measured using the VNMR command, dres) as compared to their widths in the slow-exchange limit (0 °C).[21] Values and confidence intervals for $\Delta H^‡$, $\Delta S^‡$, and $\Delta G^‡$ were determined from linear regression analysis of $\ln(k/T)$ vs $1/T$, and are reported at the 90% confidence level (Table 6).

For complex **10**, spectra were recorded over the temperature range 78.5−132.5 °C, and referenced to a spectrum collected at 23 °C. Complete line shape analysis (CLSA)[22] of these spectra converged for an exchange protocol including only diastereomer interconversion via anion racemization (Scheme 2), but failed to converge at all temperatures when a rate parameter for ion pair reorganization was included. Coalescence of the *i*-Pr bridge methyl signals at δ 1.61 (Me_R) and δ 1.65 (Me_r) of the two diastereomers was observed at 127.5 °C.

DNMR Studies of Ion Pair Reorganization/Symmetrization in 8, 9. Ion pairs **8** and **9** were prepared in situ from $[Me_2C(Cp)(Flu)]ZrMe_2$ (**1**, 3.9 mg, 10 μmol for **8**, or 1.0 mg, 2.5 μmol for **9**) and $B(2\text{-}C_6F_5C_6F_4)_3$ (**4**, 4.8 mg, 5.0 μmol) or $Ph_3C^+B(C_6F_5)_4^-$ (2.3 mg, 2.5 μmol) with 0.5 mL of *o*-xylene-d_{10}. Decomposition of **8** begins at ∼80 °C. Complex **8** also decomposes rapidly in toluene at 115 °C on a time scale of ∼10 min to give a deep blue-purple precipitate. Immediate decomposition of **9** was detected at 80 °C and broadening of the diastereotopic methyl signals on the *i*-Pr bridge could not be clearly observed.

Concentration Dependence Study of Propylene Polymerization Catalyzed by 1 + 3. Polymerization experiments were carried out in 100 mL toluene solutions in the high-pressure reaction vessel as described above. The catalytically active species was freshly generated in 2−10 mL of dry toluene using $[Me_2C(Cp)(Flu)]ZrMe_2$ samples (**1**, 1.0 mg, 2.5 μmol; 2.0 mg, 5.1 μmol; 4.0 mg, 10 μmol; 8.0 mg, 20 μmol; 16.0 mg, 40.8 μmol; 32.0 mg, 81.6 μmol) activated with 1.0 equivalents of $B(C_6F_5)_3$ (**3**).

Propylene Polymerization Catalyzed by 1 + 3 with Added $Li^+ MeB(C_6F_5)_3^-$. Polymerization experiments were carried out in 100 mL toluene solutions in the high-pressure reaction vessel described above. $Li^+ MeB(C_6F_5)_3^-$ was prepared in situ by mixing a 1:1 molar ratio of dry LiMe powder and $B(C_6F_5)_3$ in toluene, and the mixture was shaken vigorously at room temperature for 30 min before use. ^{1}H NMR (C_7D_8, 23 °C): δ 0.79 (s, 3 H, Me). ^{19}F NMR (C_7D_8, 23 °C): δ −136.84 (d, br, $J_{F-F} = 23.0$ Hz, 6 F), −159.39 (t, $J_{F-F} = 19.6$ Hz, 3 F), −163.03 (t, $J_{F-F} = 19.6$ Hz, 6 F). The catalytically active species was freshly generated in 2∼4 mL toluene, as described above. The mixture was then combined with the corresponding $Li^+ MeB(C_6F_5)_3^-$ solution in toluene, shaken vigorously at room temperature for 3 min, and then injected immediately into the polymerization reactor.

Propylene Polymerization Catalyzed by 1 + MAO (2). Polymerization experiments were carried out in the high-pressure reaction vessel described above. In a typical polymerization, $[Me_2C(Cp)(Flu)]ZrMe_2$ (**1**, 3.9 mg) and MAO (**2**, 40 mg) were loaded in the glovebox into a septum-capped vial, to which 4 mL of toluene was added. The mixture was shaken vigorously at room temperature for 20 min before use. In the polymerization reaction flask, MAO (**2**, 80 mg) was loaded with 50 mL of toluene. The solution was then equilibrated at the desired polymerization temperature and pressure as described above.

Results and Discussion

The following analysis couples complementary methods for studying ion pairing effects in polymerization systems, and is presented in three parts. First, a description of the preparation and characterization of the in situ generated and isolated active catalytic species is presented, with detailed structural and solution/dynamic characterization of **7** and **10**, with a discussion extending these results to polymerization behavior. Second, a detailed examination is presented of the effects of varying the cocatalyst/counteranion on polymerization dynamics and product polymer characteristics, as functions of temperature, monomer concentration, and solvent. Using these results, a comparative kinetic treatment is derived which provides a self-consistent model for the effects of ion pairing/counteranion identity on polymerization behavior and product polymer attributes. Finally, we present an examination of putative catalyst and counteranion concentration effects on syndioselection and other product polymer characteristics.

This discussion focuses on the importance of ion-pairing dynamics. The cation−anion interaction is recognized to have both electrostatic and covalent components;[23,24] thus the *potential barrier* to ion pair reorganization in the isolated catalyst systems discussed below, or analogous site epimerization processes operative during polymerization, may have both electrostatic and covalent/coordinative components. Although there are doubtless differences in the relative magnitudes of the coordinative/covalent and electrostatic contributions to the ion pair reorganization barrier among the various ion pair complexes studied here, we do not distinguish between these components

(21) (a) Sandstrom, J. *Dynamic NMR Spectroscopy*; Academic Press: New York, 1982; pp 77−92, and also see ref 4a. (b) Here k is the rate constant in s^{-1}; $\Delta W = W_2, - W_1$, where W_2 is line width at half-height of the exchange broadened peak in Hz, and W_1 is the line width in the absence of exchange (the no-exchange limit, 0 °C for **7** and 23 °C for **10**). The corresponding free energies of activation can also be derived using $\Delta G^‡ = - RT[\ln(k/T) + \ln(h/k)]$.

(22) Budzelaar, P. H. M. *gNMR v. 4.1.0*; Adept Scientific plc, 1999

(23) Strauss, S. H. *Chem. Rev.* **1993**, *93*, 927−942.

(24) (a) Lanza, G.; Fragala, I. L.; Marks, T. J. *Organometallics* **2002**, *21*, 5594−5612. (b) Lanza, G.; Fragala, I. L.; Marks, T. J. *Organometallics* **2001**, *20*, 4006−4017. (c) Lanza, G.; Fragala, I. L.; Marks, T. J. *J. Am. Chem. Soc.* **2000**, *122*, 12 764−12 777.

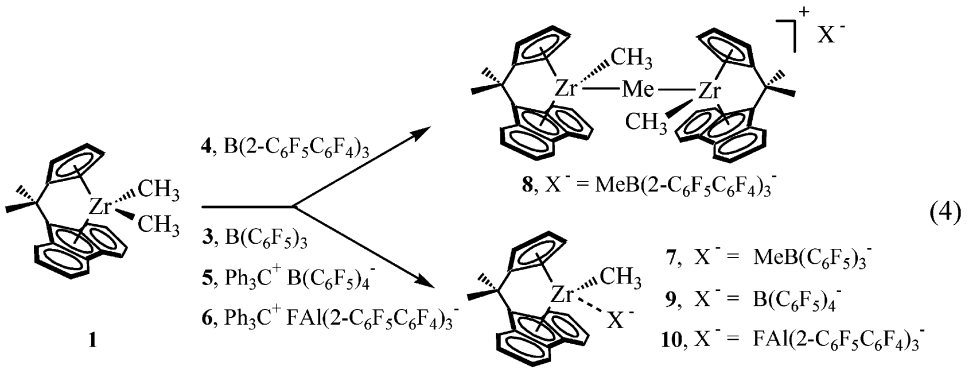

(4)

using the present experimental results, and refer to kinetic inertness of the ion pair toward reorganization as "ion pairing strength," or "coordinative tendency."

I. Zirconocenium Cations Generated via Reaction of [Me$_2$C(Cp)(Flu)]ZrMe$_2$ with Cocatalysts 3−6. The substantial body of available structural and spectroscopic data on complexes **7**−**10** permits qualitative and quantitative evaluation of cation−anion interactions. These interactions exhibit diverse structural/dynamic behavior, which is quantified using X-ray diffraction and dynamic NMR spectroscopy. The purpose of the following discussion is to highlight key structural and kinetic features of these systems, and to set the stage for correlation with polymerization characteristics.

A. Synthesis and Spectroscopy. Under rigorously anhydrous/anaerobic conditions, [Me$_2$C(Cp)(Flu)]ZrMe$_2$ (**1**) undergoes reaction with B(C$_6$F$_5$)$_3$ (**3**), B(2-C$_6$F$_5$C$_6$F$_4$)$_3$ (**4**),[8a] Ph$_3$C$^+$B(C$_6$F$_5$)$_4^-$ (**5**), and Ph$_3$C$^+$FAl(2-C$_6$F$_5$C$_6$F$_4$)$_3^-$ (**6**)[8a] to generate the corresponding ion pairs (**7**−**10**; eq 4) and to afford highly active olefin polymerization catalysts.[25] Except for **9**, these ion pairs can be isolated and characterized by standard 1-D and 2-D ^{1}H/^{19}F NMR, and analytical techniques (see Experimental Section for details); **7** and **10** have been further characterized by single-crystal X-ray diffraction (vide infra). The reaction of cocatalyst B(C$_6$F$_5$)$_3$ (**3**) or Ph$_3$C$^+$FAl(2-C$_6$F$_5$C$_6$F$_4$)$_3^-$ (**6**) with **1** cleanly generates the monomeric ion pairs **7** and **10** in good isolated yield. In contrast, B(2-C$_6$F$_5$C$_6$F$_4$)$_3$ (**4**) preferentially yields cationic μ-Me bridged dinuclear complex **8** as diastereomers in a ratio of 1.8:1 (**D** and **E**, depicted below), even with stoichiometric excesses of reagent **4** and long reaction times.[8a] The reaction of cocatalyst Ph$_3$C$^+$B(C$_6$F$_5$)$_4^-$ (**5**) with **1** affords ion pair **9** as suggested by ^{1}H NMR (along with 1.0 stoichiometric equivalents of Ph$_3$CCH$_3$), with **9** being the least stable of the present four ion pairs. Attempts to isolate or crystallize this complex have been unsuccessful, and have resulted in dark oily residues and a yellow-green solution (similar behavior is observed for most known group 4 metallocenium B(C$_6$F$_5$)$_4^-$ complexes).[7c]

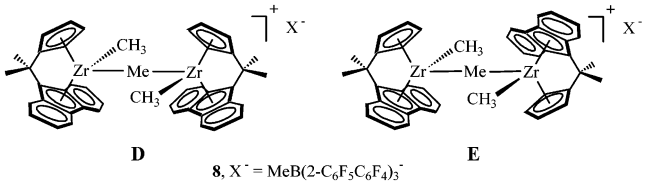

(25) NMR-scale reaction of **1** with MAO is not amenable to interpretation, thus will not be discussed here.

Interactions between the cationic and anionic portions of ion-pair complexes **7**−**10** can be evaluated qualitatively from ambient temperature 1-D ^{1}H and ^{19}F NMR spectroscopy. The ^{1}H NMR spectra of these compounds are straightforward, with four distinct resonances at δ 4−6 ppm for the C$_5$H$_4$ ring and two methyl signals at δ 1.5−2.0 ppm for the *ansa*-isopropyl group, in accord with the dissymmetry generated by the ion pairing. The Zr−C*H*$_3$ proton signals in **7**, **9**, and **10** invariably appear at $\sim\delta$ −1 ppm; in contrast, the Zr−C*H*$_3$ signals of **8** appear at −1.21 and −1.27 (for major and minor diastereomers, respectively), and the μ-Me (bridging Zr−C*H*$_3$−Zr) proton resonance of **8** appears in the region typical of this chemical environment (δ −3.33 ppm). As previously shown, metallocenium cation-MeB(2-C$_6$F$_5$C$_6$F$_4$)$_3^-$ interactions are considerably weaker than those involving MeB(C$_6$F$_5$)$_3^-$, and the equilibrium solution structure of **8** argues that neutral [Me$_2$C(Cp)(Flu)]ZrMe$_2$ has a greater affinity for the cation than does MeB(2-C$_6$F$_5$C$_6$F$_4$)$_3^-$.[5a,8a] Thus, the relative coordinative tendency of these methyl fluoroarylborate anions versus neutral [Me$_2$C(Cp)(Flu)]ZrMe$_2$ with respect to the [Me$_2$C(Cp)(Flu)]ZrMe$^+$ cation follows the order MeB(C$_6$F$_5$)$_3^-$ > [Me$_2$C(Cp)(Flu)]ZrMe$_2$ > MeB(2-C$_6$F$_5$C$_6$F$_4$)$_3^-$.

In a prior communication, we observed that ion pairing interactions between metallocenium cations and fluoroaryl counteranions significantly influence fluoroaryl ^{19}F NMR chemical shifts.[8a] Thus, the ^{19}F spectrum of complex **9** shows no substantial chemical shift differences from that of Ph$_3$C$^+$ B(C$_6$F$_5$)$_4^-$ (**5**) at room temperature, suggesting that B(C$_6$F$_5$)$_4^-$ coordination to Zr$^+$ is weak and labile. Conversely, chemical shift evidence for strong cation−anion interactions in **10** in solution is readily detected in the ^{19}F NMR spectra. Although Ph$_3$C$^+$ FAl(2-C$_6$F$_5$C$_6$F$_4$)$_3^-$ (**6**) exhibits seven ^{19}F signals (1:1:1:1:2:2), **10** exhibits nine fluoroaryl signals, indicative of restricted internal C$_6$F$_5$ rotation but free anion rotation about the Zr−F−Al linkage. The existence of **10** as diastereomers in toluene-d_8 solution, together with other structural and dynamic data, demonstrates that the mutual *o*-perfluorobiphenyl group orientations impart chirality to the Al center in solution, as seen in the solid state (vide infra). The ^{19}F NMR spectrum of **10** exhibits a characteristic broad *F*−Al resonance at δ −132.2 ppm, which, compared to the *F*−Al chemical shift of Ph$_3$C$^+$ FAl(2-C$_6$F$_5$C$_6$F$_4$)$_3^-$ (δ −175.60 ppm), demonstrates a strong M$^+\cdots$F−Al− interaction, and is consistent with a (time-averaged) preferred orientation of the fluoroaluminate ion with respect to the cation. Diffraction data clearly confirm the coordination of the FAl(2-C$_6$F$_5$C$_6$F$_4$)$_3^-$ anion via the Zr−F−Al bridge in the solid-state structure of **10**.

Table 2. Selected Bond Distances (Å) and Angles (deg) for Complex **7**

bond distances (Å)							
B−C1B	1.652(7)	Zr−C1B	2.521(4)	C1−Zr	2.248(4)	C2−Zr	2.480(4)
C7−Zr	2.615(4)	C8−Zr	2.652(4)	C13−Zr	2.524(4)	C14−Zr	2.414(4)
C18−Zr	2.429(4)	C19−Zr	2.446(4)	C20−Zr	2.521(4)	C21−Zr	2.515(4)
C22−Zr	2.433(4)	C14−C15	1.553(6)	C15−C18	1.512(6)	B−C35	1.650(7)
B−C29	1.651(7)	B−C23	1.669(7)	C24−F2	1.366(6)		

bond angles (deg)					
B−C1B−Zr	165.5(3)	C1−Zr−C1B	94.15(17)	C1B−B−C23	108.2(4)
C1B−B−C35	107.7(4)	C1B−B−C29	110.1(4)	C29−B−C23	107.1(4)
C35−B−C23	112.8(4)	C35−B−C29	111.0(3)	C14−C15−C18	99.5(3)
C16−C15−C17	106.2(4)	C14−Zr−C18	57.76(15)		

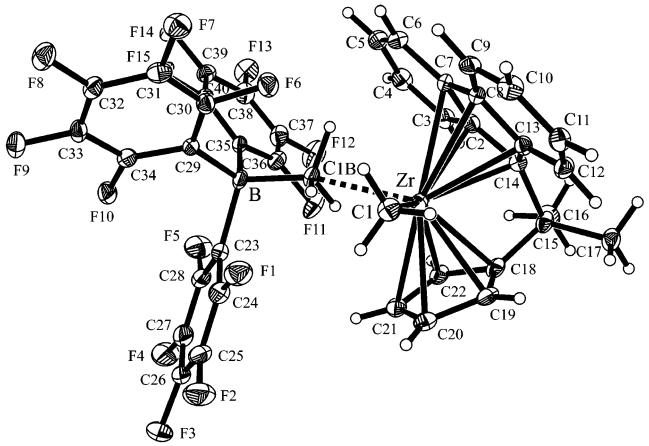

Figure 2. Perspective ORTEP drawing of the molecular structure of the complex $[Me_2C(Cp)(Flu)]ZrMe^+$ $MeB(C_6F_5)_3^-$ (**7**). Thermal ellipsoids are drawn at the 30% probability level.

B. X-ray Crystal Structures of $[Me_2C(Cp)(Flu)]ZrMe^+$ $MeB(C_6F_5)_3^-$ (7), and $[Me_2C(Cp)(Flu)]ZrMe^+$ $FAl(2\text{-}C_6F_5\text{-}C_6F_4)_3^-$ (10). Attempts were made during the course of this study to grow single-crystal samples of complexes **7**−**10**, and crystals of more stable ion pairs **7** and **10** suitable for X-ray analysis were obtained.[26] The structure of **7** shows the $[Me_2C(Cp)(Flu)]ZrMe^+$ cation in contact with the counteranion through the $MeB(C_6F_5)_3^-$ methyl group (Figure 2). Important bond distances and angles for **7** are summarized in Table 2. The Zr−Me_B−B bridge is nearly linear (bond angle 165.5(3)°). This interaction has been shown by ab initio calculations to be predominantly electrostatic in nature.[24] The Me_B−Zr-Me_M bond angle is 94.15(17)°, with the Zr−Me_M distance (2.248(4)Å), significantly shorter than the Zr−Me_B distance (2.521(4)Å). In comparison with the noncoordinating $Me_BB(C_6F_5)_3^-$ anion in previously reported structure $\{([Me_2C(Cp)(Flu)]Zr(C_6F_5))_2(\mu\text{-}F)\}^+$ $MeB(C_6F_5)_3^-$,[8a] the slightly longer Me_B−B bond distance (1.652(7)Å vs 1.64(2)Å) and smaller mean $C(C_6F_5)$−B−Me_B angle (108.7(4)° vs 111.4(9)°) show the effect on anion structure in **7** due to cation−anion interaction. This observed coordination-induced lengthening of the B−Me_B bond and flattening of the $B(C_6F_5)_3$ substructure (compared to uncoordinated $MeB(C_6F_5)_3^-$) possibly reflect the degree to which the cation and anion share the Me_B moiety, hence the degree of covalent character of the Zr−Me_B interaction. In comparison with reported analogous zirconocenium $MeB(C_6F_5)_3^-$ ion pair crystal structures (**F**−**J**),[27a−e] the present result affords the shortest B-Me_B (0.024Å shorter than the average of **F**−**I**)[27f] and Zr−Me_B bond distances observed to date (0.047 Å shorter than the average), and the largest mean $C(C_6F_5)$−B−Me_B angle (1.8° larger than the average; Table 3), suggesting that the covalent character of the action-anion interaction, whereas evident, is least in the present case.

The observed Cp(centroid)−Zr−Cp(centroid) angle (bite angle) for **7** (118.6°), as compared with **F** (127.0°),[27a] may be correlated with closer proximity of the bridging methyl carbon and counteranion boron atoms to the metal in structure **7**. However, the steric bulk of the ancillary ligand structure and difference in backbone composition in **F** also possibly contribute to the observed differences in Zr−Me_B−$B(C_6F_5)_3$ geometry.

The crystal structure of **10** shows the $[Me_2C(Cp)(Flu)]ZrMe^+$ moiety in close contact with sterically congested $FAl(2\text{-}C_6F_5C_6F_4)_3^-$ through a Zr−F−Al bridge (Figure 3). Important bond distances and bond angles of **10** are summarized in Table 4. For **10**, the Zr−F−Al (162.21(10)°) and F−Zr−Me (92.65(10)°) bond angles, as well as the Zr−Me (2.245(3)Å) and Al−F (1.7858(17)Å) bond distances are reminiscent of those in $[rac\text{-}Me_2Si(Ind)_2ZrMe]^+$ $FAl(2\text{-}C_6F_5C_6F_4)_3^-$ (166.5(8)°, 90.8(6)°, 2.24(2)Å, 1.81(1)Å, respectively).[8a] The anion in **10** adopts a pseudotetrahedral geometry, with the C_6F_5−C_6F_4 torsion angles substantially divergent from 90° (72.3° on average; ranging from 70.6° to 79.0°). In comparison with trityl salt **6**, which shows no cation−anion coordinative interaction in the solid state,[8a] **10** exhibits a much longer Al−F bond distance (1.786(2)Å vs 1.682(5)Å) and much smaller average of the three F−Al−$C_{12}F_9$ bond angles (103.0(1)° vs 107.7(3)°), demonstrating that the impact of the zirconocenium cation on the structure of the fluoroaluminate anion is large in comparison to the cation influence on the anion structure in **7**.

Direct comparison of the cation structures in complexes **7** and **10** shows a subtle relationship between counteranion identity and Zr environment. In **10**, the larger Cp(centroid)-Cp(flu, centroid) distance (3.796(11)Å vs 3.763(14)Å), greater metal−

(26) When a toluene solution of complex **7** was left standing at room temperature for two weeks, crystals of decomposition product $\{[Me_2C(Flu)(Cp)Zr(C_6F_5)]_2(\mu\text{-}F)\}^+$ $MeB(C_6F_5)_3^-$ were obtained, as reported previously, see ref 8a.

(27) (a) **F**, $[Me_2Si(Cp')_2]ZrMe^+$ $MeB(C_6F_5)_3^-$; Cp′ = $C_5H_2(Me)(t\text{-}Bu)$, ref 14. (b) **G**, $(Cp)_2ZrMe^+MeB(C_6F_5)_3^-$, Guzei, I. A.; Stockland, R. A.; Jordan, R. F. *Acta Crystallogr., Sect. C (Cryst. Str. Comm.)* **2000**, *C56*, 635−636. (c) **H**, $[Me_4C_2(Cp)_2]ZrMe^+$ $MeB(C_6F_5)_3^-$, Beck, S.; Prosenc, M. H.; Brintzinger, H. H.; Goretzki, R.; Herfert, N.; Fink, G. *J. Mol. Catal. A: Chem.* **1996**, *111*, 67−79. (d) **I**, $[(1,3\text{-}C_5H_3R_2)_2]ZrMe^+$ $MeB(C_6F_5)_3^-$; R = $SiMe_3$, ref. 4a, also see: Bochmann, M.; Lancaster, S. J.; Hursthouse, M. B.; Malik, K. M. A. *Organometallics* **1994**, *13*, 2235−2243. (e) **J**, $[(1,2\text{-}C_5H_3Me_2)_2]ZrMe^+$ $MeB(C_6F_5)_3^-$, ref. 4a. (f) Average of the five complexes, **F**−**J**.

Table 3. Comparison of Selected Bond Distances (Å) and Angles (deg) in Complex **7** to Those of Analogous Zirconocenium−$MeB(C_6F_5)_3^-$ Ion Pairs[27]

Complex	**F**[27a]	**G**[27b]	**H**[27c]	**I**[27d]	**J**[27e]	Average[a]	**7**
Cation Structure	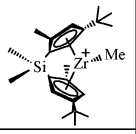		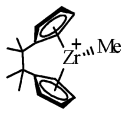	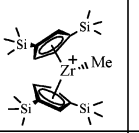			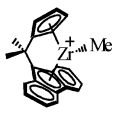
$Zr–Me_M$	2.294(8)	2.251(3)	2.258(9)	2.260(4)	2.252(4)	2.263(20)	2.248(4)
$Zr–Me_B$	2.550(8)	2.556(2)	2.516(8)	2.667(5)	2.549(3)	2.568(60)	2.521(4)
$B–Me_B$	1.688(13)	1.667(3)	1.678(12)	1.684(7)	1.663(5)	1.676(10)	1.652(7)
$B–(C_6F_5)_3$[b]	1.657(12)	1.656(8)	1.648(11)	1.704(14)	1.652(11)	1.664(23)	1.657(11)
$Zr–Me_B–B$	162.7(6)	169.1(2)	171.5(5)	170.5(3)	161.8(2)	167.1(45)	165.5(3)
$Me_M–Zr–Me_B$	92.4(3)	87.7(9)	91.8(3)	97.1(1)	92.0(1)	92.2(33)	94.2(2)
$Me_B–B–(C_6F_5)_3$[c]	109.0(49)	108.8(44)	107.8(44)	109.0(27)	108.0(50)	108.5(6)	110.3(29)
Cp–Zr–Cp[d]	127.0	131.1	125.1	132.4	131.3	129.4	118.6

[a] Average of structures **F**−**J**. [b] Mean B−C(C_6F_5) distance. [c] Mean Me_M−B−C(C_6F_5) angle. [d] Bite angle.

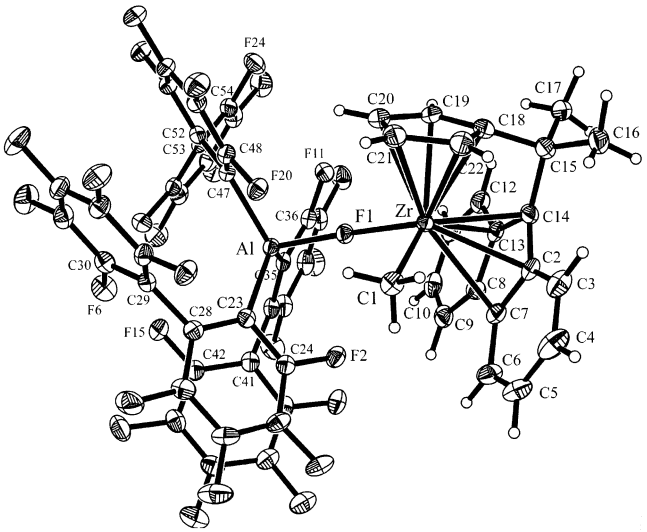

Figure 3. Perspective ORTEP drawing of the molecular structure of the complex $[Me_2C(Cp)(Flu)]ZrMe^+$ $FAl(2\text{-}C_6F_5C_6F_4)_3^-$ (10). Thermal ellipsoids are drawn at the 30% probability level. The terminal C_6F_5 groups not only twist out of coplanarity with connected C_6F_4 fragments but also exhibit $\pi-\pi$ interactions with the C_6F_4 groups on adjacent $C_{12}F_9$ ligands.

ligand distances (Zr−Cp(centroid), 2.176(3)Å vs 2.157(4)Å; Zr−C(*i*-Pr bridging), 3.124(3)Å vs 3.109(4)Å), and greater C(bridgehead, Cp)-C(*i*-Pr bridging) bond distance (1.530(5)Å vs 1.512(6)Å) in **10**, reveal: (a) that the Zr center is displaced slightly out of the $[Me_2C(Cp)(Flu)]^{2-}$ ligand pocket in **10** as compared to **7**, and (b) that the $[Me_2C(Cp)(Flu)]^{2-}$ ligand is pried open by $FAl(2\text{-}C_6F_5C_6F_4)_3^-$. The above observations indicate a stronger coordinative interaction with the bulkier but more strongly donating $FAl(2\text{-}C_6F_5C_6F_4)_3^-$ anion (Table 5). Note that in **10**, $\pi-\pi$ stacking is also observed among the $C_{12}F_9$ groups of the anion, where the C_6F_4 rings bound to the Al center engage in stacking with the end C_6F_5 rings on adjacent $C_{12}F_9$ groups. The sense of the corkscrew motif described by the $C_{12}F_9$ groups determines the stereochemical configuration at the Al center. In contrast, this $\pi-\pi$ stacking interaction is conspicuously absent in the solid-state structure of trityl salt **6**. This, together with the observed interconversion of diastereomers of **10** in solution (vide infra), suggests a subtle reciprocation between ancillary ligand architecture and structural dynamics.[8a]

C. Solution Dynamics of Ion Pair Reorganization/Symmetrization in $[Me_2C(Cp)(Flu)]ZrMe^+$ $MeB(C_6F_5)_3^-$ (7) and $[Me_2C(Cp)(Flu)]ZrMe^+$ $FAl(2\text{-}C_6F_5C_6F_4)_3^-$ (10). Exchange processes available to ion pairs **7** and **10** in the absence of olefin can be correlated with polymerization behavior of these catalyst systems. The principal structural reorganization process of interest in each of these systems is migration of the anionic portion of the catalyst-cocatalyst system from one side of the zirconocenium-methyl metal center to the other (ion pair reorganization). This process mirrors the site epimerization of the zirconocenium-polymeryl-anion ensemble thought to occur during polymerization and to give rise to product *m* stereodefects in the absence of synchronous propylene enchainment (eq 2; Scheme 1B). In the absence of olefin, both **7** and **10** undergo background exchange processes as well, and ion pair reorganization must be studied in the context of all extant reorganization processes.

Table 4. Selected Bond Distances (Å) and Angles (deg) for Complex **10**

bond distances (Å)							
Al−F1	1.7858(17)	F1−Zr	2.1165(15)	C1−Zr	2.245(3)	C2−Zr	2.531(3)
C7−Zr	2.621(3)	C8−Zr	2.594(3)	C13−Zr	2.498(3)	C14−Zr	2.419(3)
C18−Zr	2.444(3)	C19−Zr	2.451(3)	C20−Zr	2.530(3)	C21−Zr	2.538(3)
C22−Zr	2.460(3)	C14−C15	1.554(4)	C15−C18	1.530(5)	Al−C23	2.014(3)
Al−C35	2.012(3)	Al−C47	2.025(3)	C28−C29	1.497(4)	C24−F2	1.369(3)

bond angles (deg)					
Al−F1−Zr	162.21(10)	F1−Zr−C1	92.65(10)	F1−Al−C23	103.52(10)
F1−Al−C35	100.14(10)	F1−Al−C47	105.32(10)	C35−Al−C23	116.00(12)
C35−Al−C47	115.34(12)	C23−Al−C47	113.98(12)	C18−C15−C14	99.5(2)
C16−C15−C17	106.5(3)	C14−Zr−C18	57.89(10)	C23−C28−C29	123.2(3)

Table 5. Comparative Bond Distances (Å) and Angles (deg) for Complexes **7** and **10**

	Zr−C_{Flu}[a]	Zr−C_{Cp}[b]	Zr−C_{15}	C_{Cp}−Zr−C_{Flu}	C_{15}−C_{14}	C_{15}−C_{18}	C_{14}−C_{15}−C_{18}
7	2.221(4)	2.157(4)	3.109(4)	118.6(2)	1.553(4)	1.512(6)	99.5(3)
10	2.221(3)	2.176(3)	3.124(3)	119.0(1)	1.554(4)	1.530(5)	99.5(2)

[a] Centroid of $C_{13}H_8$ ligand. [b] Centroid of C_5H_4 ligand.

The ^{1}H EXSY spectrum of ion pair **7** at 23 °C shows NOE contact between protons Me_B and H_F (see atom labeling scheme **C** in Experimental Section), with sufficient intensity to indicate that the time-averaged solution structure of **7** is a dissymmetric contact ion pair, with a preferred orientation of the anion with respect to the cation.[28] This spectrum reveals exchange between Me_B and Me_M signals (methyl-methide exchange), arising from borane migration (dissociation of $B(C_6F_5)_3$ from Me_B and subsequent transfer to Me_M) and also permutation of diastereotopic Me_R and $Me_{R'}$ resonances and exchange between corresponding fluorenyl and cyclopentadienyl ring proton pairs (ligand side-side exchange, arising from both borane migration and ion pair reorganization, eq 5). Relative rates of borane migration and ion pair reorganization are sensitively dependent on metal identity and ligand architecture, as shown in previous studies of archetypal Group 4 metallocene dimethyl precatalysts activated with $B(C_6F_5)_3$.[4a,12,29]

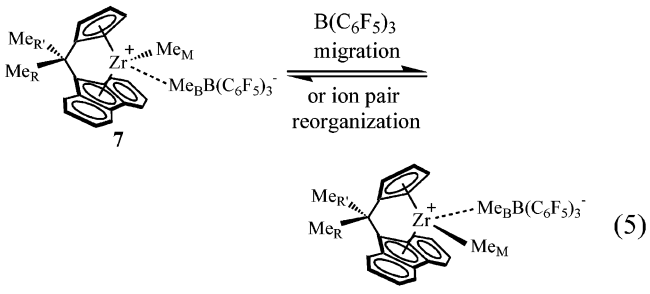

(5)

1-D ^{1}H NMR spectral data collected for **7** over a 40° temperature range afford kinetic parameters for both of these processes. Broadening of the *i*-Pr methyl (Me_R and $Me_{R'}$) and methide resonances (Me_M) can be used to determine the rates of both processes using the standard modified Bloch two-site exchange line-broadening formalism, $k = \pi(\Delta W)$.[21b] At a given temperature, the ion pair reorganization rate is taken as the difference between total side-side exchange rate, taken from broadening in the Me_R and $Me_{R'}$ resonances, and the rate of borane migration, determined from broadening of Me_M.[30] Kinetic results are summarized in Table 6. Confidence intervals for $\Delta H^‡$ and $\Delta S^‡$ are determined using standard error values from linear regression analysis on the data used to generate the Eyring plot.

Table 6. NMR-Derived Rate Constants and Free Energies of Activation for Solution Dynamic Processes of Complexes **7** and **10** in Toluene-d_8[j]

cocat. (cat.)	*T* (°C)	k_{total}[a] (s^{-1})	k_1 (s^{-1})	$\Delta G_1^‡$ (kcal/mol)	k_{reorg}[d] (s^{-1})	$\Delta G_{reorg}^‡$ (kcal/mol)
3(**7**)[e]	77.5	6.0	5.2[b]	19.6(10)	0.8(4)	20.6(36)
3(**7**)[e]	92.5	18.6	16.4[b]	19.4(10)	2.2(4)	20.8(36)
6(**10**)[e]	87.5	1.1	1.1[c]	21.2(6)	∼0[g]	n.d.
6(**10**)[f]	87.5	2.8	2.8[c]	20.5	∼0[g]	n.d.
6(**10**)[h]	117.5	8.4	8.4[c]	21.4(6)	∼0[g]	n.d.
6(**10**)[f]	117.5	18.3	18.3[c]	20.8	∼0[g]	n.d.
6(**10**)[e]	127.5	15.0	15.0[c]	21.5(6)	∼0[g]	n.d.
6(**10**)[f]	127.5	n.d.[i]	n.d.[i]	n.d.[i]	<0.25	>24.8

[a] $k_{total} = k_1 + k_{reorg}$. [b] For **7**, k_1 = rate constant for $B(C_6F_5)_3$ migration. [c] For **10**, k_1 = rate constant for anion racemization. [d] k_{reorg} = rate constant of ion pair reorganization. [e] Taken from line-broadening analysis. [f] From 2D-EXSY NMR. [g] Assumed based on EXSY results at 127.5 °C. [h] Projected values from line-broadening analysis. [i] Anion racemization saturation regime, see discussion. [j] Confidence intervals presented at the 90% confidence level.

Exchange-broadening observed in variable-temperature 1-D ^{1}H spectra of **10** arises from two discrete processes: ion pair reorganization, and interconversion between stereochemical configurations at the chiral Al center (anion racemization, see Scheme 2 for both processes). Both processes interconvert major and minor diastereomers, however ion pair reorganization does so with ligand side-side exchange, whereas anion racemization does not. Thus EXSY can be used to differentiate between them. EXSY spectra collected at 23 °C, 87.5 °C, and 117.5 °C (τ_m = 1200 ms, 185 ms, 40 ms, respectively) exhibit cross-peaks corresponding to interconversion between diastereomers, but no cross-peak intensity indicative of ligand side exchange. This observation motivated EXSY data collection at 127.5 °C (τ_m = 800 ms) specifically to examine the possibility of very slow ion pair reorganization. This spectrum also reveals no apparent side-side exchange cross-peak intensity (Figure 4), and is analyzed to establish a lower limit for the ion pair reorganization

(28) Zuccaccia, C.; Stahl, N. G.; Macchioni, A.; Chen, M.-C.; Roberts, J. A.; Marks, T. J. *J. Am. Chem. Soc.* **2004**, *126*, 1448−1464.

(29) Line broadening is found to be independent of concentration over an 8-fold range for **7**, arguing that an intramolecular exchange process is prevalent.

(30) Temperature-dependent quadrupolar broadening of the Me_B resonance precludes measurement of exchange broadening on this signal, which is instead assumed to be equal to that of the Me_M resonance. The detection limit for broadening is determined by the digital resolution (0.067 Hz, corresponding to k = 0.21 s^{-1}), thus the site exchange rate at 23 °C ($k \approx 0.2$ s^{-1}) as determined from EXSY data demonstrates that 0 °C is a suitable temperature to take as the zero-exchange limit for the purposes of line-shape analysis.

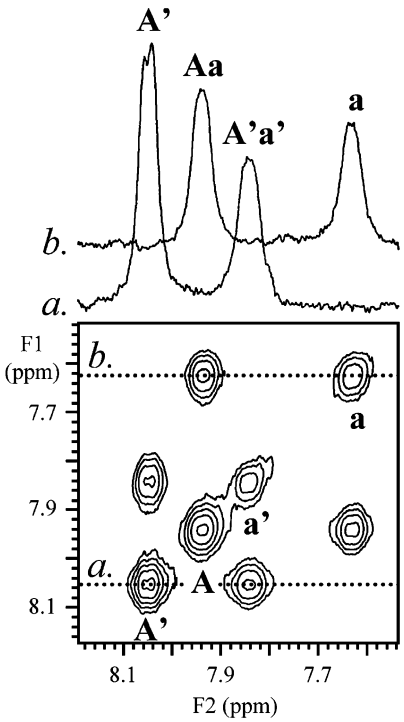

Figure 4. EXSY spectrum (in toluene-d_8) of complex **10**, 127.5 °C, τ_m = 800 ms. Diagonal peaks, lower-left to upper-right, correspond to resonances $H_{A'}$, H_A, $H_{a'}$, and H_a, respectively. Spectra *a.* and *b.* are F2 slices passing through the points of greatest intensity in resonances H_a and $H_{A'}$, respectively.

rate at this temperature. In Figure 4, Aa and aA, or collectively [Aa], refer to the pair of H_A-H_a exchange peaks (see atom labeling scheme **C** in the Experimental Section), and $I_{Aa} = I_{aA}$ refers to the cross-peak intensity at these positions.[31] Cross-peaks at [Aa], and at [A′a′] arise exclusively from anion racemization. Intensity at [Aa′], [A′a], [AA′], and [aa′] is expected from ion pair reorganization + rapid anion racemization, with only the former process permuting ligand sides. Any cross-peak intensity from ion pair reorganization is distributed over these eight locations by the background anion racemization (for which the present conditions represent the saturation regime, with $k = 28$ s^{-1} at 127.5 °C from dynamic NMR).

For two-site exchange, a suitable model for the proposed ion pair reorganization under saturation conditions for anion racemization, rates is given by eq 6.[19]

$$k = \frac{1}{\tau_m}\ln\left(\frac{r+1}{r-1}\right) \text{ with } r = \frac{\sum I_{\text{diag}}}{\sum I_{\text{cross}}} \qquad (6)$$

A lower limit for r, r_{ll}, can be established using extant diagonal peak intensities and a suitable higher limit for the corresponding cross-peak intensities I_{cross}. What follows is a general method for estimating r_{ll} for systems undergoing two-site exchange *without* distribution of cross-peak intensity by background, saturation-regime processes for some q extant diagonal signals

$$r > r_{\text{ll}} \approx \frac{\sum_{\text{i}}^{q} I_{d,i}}{qI_n} = \frac{\sum_{i}^{q} \phi_{d,i} n}{q\phi_n n} = \frac{\sum_{\text{i}} \phi_{d,\text{i}}}{q\phi_n} \qquad (7)$$

(31) Signal overlap precludes use of other sets of signals for this determination.

$S_{d,i}$ with intensities $I_{d,i}$ and cross-peak intensity limit I_n, where $\Phi_{d,i}$ is the measured signal-to-noise ratio of signal $S_{d,i}$ over the (noise) region where a corresponding cross-peak is sought, and Φ_n is the arbitrary signal-to-noise ratio limit below which real intensity might be mistaken for background noise. Not all observed diagonal peaks need be employed, but for each pair of cross-peaks sought, both corresponding diagonal peaks are measured, pairing each cross-peak region with a diagonal peak, as dictated by the F2 dimension direction, when the exchange interconverts species that are present in unequal concentrations. The above formulation effectively averages the noise intensity for the q regions measured and is valid inasmuch as the noise intensity is constant across the noise regions used to measure the $\Phi_{d,i}$'s.

In the present case, diagonal peaks A′ and a give intensities $I_{A'}$ and I_a with signal-to-noise ratios $\Phi_{A'}$ (over region aA′) and Φ_a (over A′a), respectively, and $q = 2$. We extend the above general formulation to the present system using a factor D representing distribution of cross-peak intensity due to background saturation-regime exchange. Anion racemization distributes expected total cross-peak intensity such that the summed intensity of the *inter-diastereomer* cross-peaks is one-half of the total expected cross-peak intensity arising from ion pair reorganization, thus $D = 1/2$. We set the arbitrary but reasonable criterion, that a cross-peak having intensity $I_{\text{cross}} < 2\ I_n$, may be extant but indistinguishable from background noise, thus setting $\Phi_n = 2$. Supposing such a peak exists, r_{ll} is then

$$r > r_{\text{ll}} \approx D\frac{\sum_{\text{i}}^{q} \phi_{d,i}}{q\phi_n} = \frac{\phi_{A'} + \phi_a}{8} \qquad (8)$$

The signal-to-noise ratios $\Phi_{A'}$ and Φ_a (33.4 and 64.4, respectively, see Figure 4) are determined from F_2 slices passing through the highest points in A′ and a, setting $r > r_{ll} = 12.2$ and thereby giving a higher limit, $k < 0.25$ s^{-1} at 127.5 °C for ion pair reorganization, including a correction for implicit NOE intensity.[32]

Ion pair complexes formed by activation of metallocene precatalysts with Ph_3C^+ $B(C_6F_5)_4^-$ are found to be inisolable and very unstable, excepting Cp_2*$ThMe^+$ $B(C_6F_5)_4^-$.[7c] For complex **9**, determining the rate of a putative dynamic reorganization/symmetrization process analogous to that observed with **7** was unsuccessful, with extensive decomposition occurring at much lower temperatures (∼50 °C) compared to complexes **7** and **10**. Similarly, decomposition of complex **8** is observed upon heating (above ∼80 °C) and results in an insoluble, blue-purple product in toluene. It will be seen from evidence derived from polymerization results, that the site epimerization rate constant for **9** is 11.1(11) s^{-1} at 60 °C, the highest value for all systems studied, suggesting that the ion pairing interaction is weakest for $B(C_6F_5)_4^-$ as compared to the other systems (see discussion below). The structure of the active species corresponding to **8**

(32) RMS signal-to-noise ratios for specific signals over specific noise regions are obtained from the VNMR command, dsn. Scant NOE intensity detected in the EXSY spectrum of **10** at 127.5 °C at locations [A′B′], [a′b′], [A′b′], and [B′a′] (distributed by rapid anion racemization) is measured, and used together with the crystal data of **10** to estimate the expected NOE intensity at A′a and aA′ (accompanied by intensities at [Aa′], [A′A], and [a′a]) and increases the higher limit for the ion pair reorganization rate constant by 0.05 s^{-1}, assuming total cancellation of NOE and exchange cross-peak intensity at these positions.

during polymerization is unknown, however results discussed below allow an estimation of $k = 10.9(10)\ s^{-1}$ at 60 °C for a putative site epimerization in this species.

The assembled NMR-derived kinetic data (Table 6) indicate a fundamental and substantial difference in the lability of $MeB(C_6F_5)_3^-$ and $FAl(2\text{-}C_6F_5C_6F_4)_3^-$ as counteranions for the zirconocenium fragment.[33] Indeed, the lower limit derived for the barrier to ion pair reorganization in **10** is conservative, and considering that this interaction may be even stronger, it is remarkable that **10** produces polymer at all, inviting speculation on the pathway for monomer enchainment. Multiple pathways for insertion have been postulated in computational studies where the catalyst-cocatalyst interaction is included,[24] and the collection of systems presented here may serve to differentiate among these possibilities: specifically, an enchainment pathway with concerted anion displacement may be favored in the $FAl(2\text{-}C_6F_5C_6F_4)_3^-$ system, in contradistinction to the $B(C_6F_5)_4^-$ system, for example. Also, considering that monomer enchainment is in general impeded by stronger ion pairing/increasing counteranion coordinative tendencies,[12c] and that in similar systems ion pairing strength has been shown to diminish with increasing zirconocenium alkyl steric bulk,[12a] it is possible that this latter differential effect may diminish more rapidly with more strongly binding counteranions.

Independent of mechanistic considerations, differences in counteranion coordinative ability manifest themselves measurably in the rate constants for propylene insertion relative to those of competing processes believed to occur during polymerization. It is the goal of the following sections to examine these effects.

II. Catalytic Propylene Polymerization Mediated by Complexes 7−10. It will be seen that substantial counteranion effects are evident in the polymerization characteristics and polypropylene microstructures obtained using the present catalyst systems. The following sections examine cocatalyst, temperature, monomer concentration, and solvent polarity effects on stereodefect production, polymerization activity, and termination/chain-transfer kinetics. These effects represent an interplay of structural, kinetic, and thermodynamic influences, among which the dominant factor is argued to be the lability of the catalyst cation−anion interaction.

A. Counteranion and Temperature Effects on Propylene Polymerization. Under rigorously anhydrous/anaerobic conditions, complex **1** was activated with MAO (**2**) or perfluoroaryl cocatalysts **3**−**6** to generate catalytically active ion pairs in situ.[34] Polymerizations were carried out under 1.0 atm propylene pressure in toluene solution over the temperature range of −10° to 60 °C using conditions minimizing mass transfer[17] and exotherm effects (see the Experimental Section for details);[2c,10] product isolation and characterization utilized standard techniques.[11] The results of these propylene polymerization experiments are summarized in Table 7. The data are analyzed with a view toward discerning cocatalyst-dependent effects on polymerization activity, molecular weight characteristics, and microstructure, and how these may reflect the coordinative component of anion interaction with the cationic metal center.[7c] Several trends are immediately evident in the data. Product polydispersities are consistent with well-defined single-site processes and are rather temperature- and anion-insensitive. Polymer production rates, however, are highly anion-sensitive—the intrinsic steric and electronic characteristics of the anions appearing to have a major influence on monomer activation and enchainment. The most strongly ($FAl(2\text{-}C_6F_5C_6F_4)_3^-$) and weakly ($MeB(2\text{-}C_6F_5C_6F_4)_3^-$, $B(C_6F_5)_4^-$) coordinating anions generally exhibit the lowest and highest polymerization rates, respectively (Table 7). Not surprisingly,[1,11] product molecular weights fall with rising reaction temperature, in all cases (Figure 5). $FAl(2\text{-}C_6F_5C_6F_4)_3^-$ affords the highest M_w product polymer at all temperatures (vide infra for pressure effects). Most interesting, however, is the striking pattern in polypropylene stereodefect probabilities[35] (P_m, generally attributed to site epimerization,[36] Scheme 1B, and P_{mm}, from propylene enantiofacial misinsertion or chain epimerization, Schemes 1D, 1E, respectively) as a function of anion and temperature (Figure 6). It can be seen that the $FAl(2\text{-}C_6F_5C_6F_4)_3^-$-based catalyst exhibits far higher syndiospecificity, with far lower *m* and somewhat lower *mm* stereodefect production. All systems exhibit a not unprecedented erosion in syndioselectivity with increasing temperature,[11] likely due to acceleration of *m* steric dyad production vs enchainment, least prevalent in the $FAl(2\text{-}C_6F_5C_6F_4)_3^-$-based catalyst. The NMR-derived ion pair reorganization/symmetrization kinetic results and the comparatively low polymerization activity temperature dependence for **10** argue that tighter ion pairing raises the activation energy for site epimerization. Interestingly, *mm* stereodefects are far less temperature-sensitive for all catalysts, with the $FAl(2\text{-}C_6F_5C_6F_4)_3^-$ catalyst again slightly superior. In contrast, the $MeB(C_6F_5)_3^-$ catalyst exhibits the lowest syndiotacticity with greatest increase of *m* and *mm* stereodefect production with rising polymerization temperature (vide infra for detailed explanation). In general, as the temperature is increased, polymerization activities increase, except near 60 °C, where activities decrease for all ion pairs. Not only lower ion pair thermal stability, but also decreased propylene solubility at higher temperatures doubtless contributes to the lower activity observed in all systems at 60 °C (in toluene, [propylene] = 0.36 M at 60 °C vs 0.83 M at 25 °C, at 1.0 atm system pressure).[37] In addition, the $B(C_6F_5)_4^-$-derived catalyst exhibits the most significant erosion in performance, likely reflecting the poor thermal stability of this complex as noted above. In comparison to the $FAl(2\text{-}C_6F_5C_6F_4)_3^-$-based polymerization system, lower product syndiotacticities but higher polymerization activities are observed in the **1** + MAO system. In agreement with previous polymerization studies using [Me_2C-

(33) Dynamic NMR experiments with **7** and **10** 1,2-dichlorobenzene-d_4 as solvent reveal that in this more polar medium, the barrier to ion pair reorganization in **7** is lowered, whereas with **10** such a process is still undetectable.

(34) For experiments using MAO (**2**) as cocatalyst, an Al:Zr ratio of 60: 1 is employed, to improve comparability with results collected using molecular cocatalysts. Control experiments in which the Al:Zr ratio is varied across a 30-fold range show no significant dependence of the pentad distribution on this ratio. These results are presented in Table 2 of the Supporting Information.

(35) For **1** + MAO, syndiotacticity falls with increasing polymerization temperature, ref 11, while for C_1-symmetric catalysts, isotacticity sometimes increases with increasing polymerization temperature: (a) Kleinschmidt. R.; Reffke, M.; Fink, G. *Macromol. Rapid Commun.* **1999**, *20*, 284−288. (b) Grisi, F.; Longo, P.; Zambelli, A.; Ewen, J. A. *J. Mol. Catal. A: Chem.* **1999**, *140*, 225−233. (c) For an example of a C_2-symmetric catalyst propylene polymerization temperature dependent study, see: Resconi, L.; Piemontesi, F.; Camurati, I.; Sudmeijer, O.; Nifant′ev, I. E.; Ivchenko, P. V.; Kuz′mina, G. K. *J. Am. Chem. Soc.* **1998**, *120*, 2308−2321.

(36) See ref 11. Other proposed processes giving rise to *m* stereodefects are discussed below. See ref 2c.

(37) An empirical model for the calculation of the solution-phase composition of propylene in toluene and isododecane under relavent conditions is presented in (a) Dariva, C.; Lovisi, H.; Santa Mariac, L. C.; Coutinho, F. M. B.; Oliveira, J. V.; Pinto, J. C. *Can. J. Chem. Eng.* **2003**, *81*, 147−152. (b) also see ref 17.

Table 7. Propylene Polymerization Results for the Reactions Mediated by **1**+ Indicated Cocatalysts under 1.0 atm of Propylene over the Temperature Range from −10 to +60 °C[a]

cocat. (cat.)	exp. no.	T_p (°C)	cat. (μmol)	$[C_3H_6]$[b] (M)	time (s)	yield[c] (g)	$v_{p,apparent}$[d] ($M*s^{-1}$)	k_p[e] ($M^{-1}*s^{-1}$)	T_m (°C)	M_w[f] ($kg*mol^{-1}$)	P.D.I.[f]	P_m[g] (%)	P_{mm}[g] (%)	r[h] (%)	$rrrr$[i] (%)
2	1	−10	10	2.83	1800	0.77	0.188	0.36	156.0	138	1.88	0.3	0.7	98.2	95.3
	2	0	5.0	1.87	1200	0.75	0.278	1.6	151.0	139	1.85	0.4	0.9	97.8	94.1
	3	10	3.3	1.31	600	0.73	0.535	6.6	148.9	125	1.83	0.5	0.9	97.6	93.6
	4	25	3.3	0.83	600	2.20	1.61	32	141.5	124	1.88	1.3	1.4	96.1	88.7
	5	40	2.5	0.56	600	1.80	1.32	51	129.5	80.8	1.87	2.7	1.5	94.3	83.1
	6	60	2.5	0.36	1200	1.24	0.459	27[j]	N.O.[k]	36.7	2.16	8.0	2.8	87.6	63.8
3(7)[l]	7	−10	20	2.83	1800	0.50	0.122	0.12	147.0	79.8	1.75	1.3	1.4	95.8	88.6
	8	0	20	1.87	1800	1.14	0.279	0.40	140.4	78.8	1.56	2.0	1.6	94.7	85.2
	9	10	20	1.31	3600	4.68	0.572	1.2	127.3	126	1.87	3.1	1.5	93.9	81.8
	10	25	20	0.83	1800	4.40	1.08	3.5	101.4	79.0	1.81	6.7	2.0	89.7	69.0
	11	40	10	0.56	600	0.94	0.689	6.6	69.0	41.6	1.92	12	2.5	83.9	53.1
	12	60	20	0.36	1800	2.48	0.606	4.5[j]	N.O.[k]	11.9	2.38	20	4.3	74.7	34.6
4(8)	13	−10	7.6	2.83	720	0.88	0.538	1.4	150.9	201	1.83	0.5	1.3	97.3	92.9
	14	0	5.0	1.87	600	0.62	0.455	2.6	147.4	168	1.83	0.7	1.4	96.6	90.8
	15	10	5.0	1.31	300	0.69	1.01	8.4	143.2	132	1.92	1.0	1.7	95.8	88.5
	16	25	10	0.83	300	2.92	4.28	28	130.3	101	1.85	2.4	1.9	94.1	82.7
	17	40	6.2	0.56	300	3.71	5.44	84	108.2	82.8	1.78	5.3	2.6	90.6	72.4
	18	60	10	0.36	600	1.74	1.28	19[j]	N.O.[k]	53.1	1.82	13	3.2	82.0	49.5
5(9)[l]	19	−10	1.5	2.83	300	1.18	1.73	22	151.5	229	1.95	0.4	1.1	97.0	92.1
	20	0	1.3	1.87	180	0.74	1.81	40	147.6	180	1.93	0.8	1.3	96.5	90.7
	21	10	1.3	1.31	120	0.42	1.54	49	143.5	153	1.98	1.2	1.5	95.6	88.3
	22	25	1.3	0.83	180	0.73	1.78	90	130.7	112	1.95	2.4	1.9	93.8	82.4
	23	40	2.6	0.56	75	0.77	4.52	167	110.3	82.6	1.96	5.1	2.3	89.9	70.8
	24	60	10	0.36	600	1.27	0.932	14[j]	N.O.[k]	55.8	1.82	13	3.2	82.4	50.8
6(10)	25	−10	20	2.83	10 800	0.85	0.035	0.030	156.5	290	1.86	0.3	0.9	97.8	94.3
	26	0	20	1.87	3600	0.54	0.066	0.10	154.5	242	2.04	0.3	1.0	97.6	93.9
	27	10	20	1.31	4500	1.58	0.155	0.32	151.2	204	1.96	0.5	1.2	97.1	92.6
	28	25	20	0.83	4500	5.00	0.489	1.6	145.7	147	1.85	0.9	1.5	96.1	89.5
	29	40	20	0.56	3600	0.51	0.062	0.30[j]	136.0	104	2.09	1.7	2.0	94.1	84.2
	30	60	20	0.36	1800	0.25	0.061	0.45[j]	N.O.[k]	66.5	1.95	5.3	2.7	89.8	70.8

[a] In 54 mL of toluene. [b] See ref 37a. [c] After workup (see Experimental Section). [d] As calculated from polymerization yield. [e] As calculated from $v_{p,apparent}$. [f] Determined from GPC analysis relative to polystyrene standards; polydispersity index = M_w/M_n. [g] Determined from polymer ^{13}C NMR pentad analysis. [h] Fractional dyad content, $r = (\Sigma_{x,y}\ xmry + \Sigma_{x,y}\ xrmy + 2\Sigma_{x,y}\ xrry)/2$, with $x, y \in \{r, m\}$. [i] Calculated *rrrr* signal integral; see Supporting Information for experimental and calculated pentad distributions. [j] Not used for estimating k_p at 60 °C. [k] Not observed. [l] These data supplemented with additional results for estimation of k_p at 60 °C (see Supporting Information).

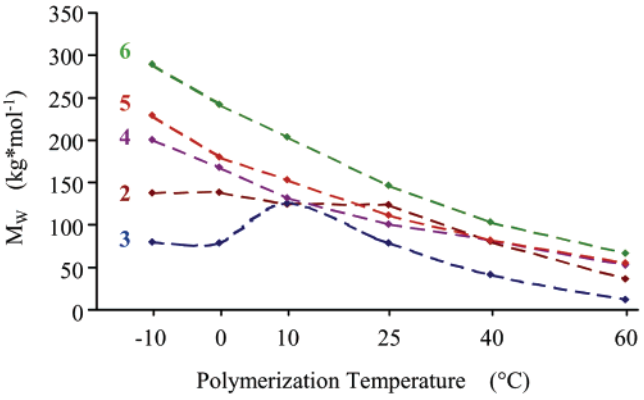

Figure 5. Product molecular weight (M_w) data for polypropylenes produced by **1**+ the indicated cocatalysts over the temperature range from −10° to +60 °C under 1.0 atm of propylene.

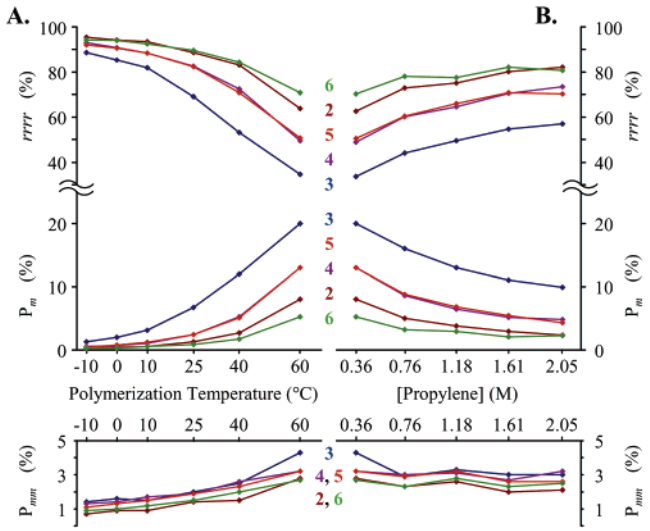

Figure 6. A. Syndiotacticity (%*rrrr*) data and calculated *m* and *mm* stereodefect production probabilities (relative to insertion, P_m and P_{mm} respectively, discussed below) for polypropylenes produced by **1**+ indicated cocatalysts under 1.0 atm of propylene over the temperature range from −10° to +60 °C.

(Cp)(Flu)]$ZrCl_2$ + MAO (% *rrrr* = 93.1 at 10 °C),[35a] comparable *rrrr* pentad contents (93.6%, Table 7, entry 3) are obtained in the present work. The temperature dependence of derived kinetic parameters will be addressed below.

B. Monomer Concentration Effects. Polymerization series in which [propylene] is systematically varied reveal anion dependences that are subtle compared to the anion sensitivity of the temperature effects described above. These experiments were carried out with T = 60 °C, to maximize signal-to-noise ratios for dilute pentad signals. The mechanistic consequences of increasing [propylene] can be ascribed to increased rates of bimolecular reactions such as insertion or enantiofacial misinsertion vs those of competing unimolecular processes such as site epimerization and β-hydrogen elimination to Zr (resulting in either chain epimerization or termination and reasonably assumed to be zero-order in monomer). Generally, any observed [propylene] effect on a measurable polymer feature can be interpreted as arising from a combination of processes having

Table 8. Propylene Polymerization Results for the Reactions Mediated by **1**+ Indicated Cocatalysts at 60 °C over the Pressure Range of 1−5 atm of Propylene[a]

cocat. (cat.)	exp. no.	*P* (atm)	cat. (μmol)	$[C_3H_6]$[b] (M)	time (s)	yield[c] (g)	$v_{p,apparent}$[d] ($M*s^{-1}$)	k_p[e] ($M^{-1}*s^{-1}$)	T_m (°C)	M_w[f] ($kg*mol^{-1}$)	P.D.I.[f]	P_m[g] (%)	P_{mm}[g] (%)	*r*[h] (%)	*rrrr*[i] (%)
2	1	1.0	2.5	0.36	1200	1.24	0.454	27	N.O.[j]	36.7	2.16	8.0	2.8	87.0	62.7
	2	2.0	1.5	0.76	240	0.92	1.69	80	113.8	48.8	1.87	5.0	2.3	90.8	72.9
	3	3.0	1.5	1.18	120	1.03	3.79	116	122.2	56.7	1.84	3.8	2.6	91.1	75.2
	4	4.0	1.5	1.61	180	1.88	4.60	103	125.4	63.2	1.81	2.9	2.0	93.2	80.2
	5	5.0	1.5	2.05	120	2.19	8.03	141	131.6	71.2	1.80	2.3	2.1	93.6	82.2
3(7)	6	1.0	20	0.36	1800	2.48	0.606	4.5	N.O.[j]	11.9	2.38	20	4.3	74.6	33.6
	7	2.0	6.6	0.76	1200	1.18	0.433	4.6	N.O.[j]	19.0	2.03	16	2.9	79.8	43.9
	8	3.0	5.9	1.18	1200	2.41	0.884	6.9	N.O.[j]	25.0	2.55	13	3.3	81.7	49.5
	9	4.0	5.9	1.61	1200	2.82	1.03	5.9	N.O.[j]	29.5	2.57	11	3.0	83.9	54.5
	10	5.0	5.1	2.05	1200	1.52	0.560	2.9	N.O.[j]	33.9	1.89	9.9	3.0	84.9	57.1
4(8)	11	1.0	10	0.36	600	1.74	1.28	19	N.O.[j]	53.1	1.82	13	3.2	81.7	48.9
	12	2.0	2.9	0.76	1200	1.31	0.480	12	N.O.[j]	53.5	1.80	8.6	3.0	86.2	60.2
	13	3.0	2.5	1.18	1200	1.88	0.689	13	99.0	55.8	1.89	6.5	3.1	87.5	64.6
	14	4.0	2.9	1.61	600	1.19	0.873	10	106.0	56.6	1.86	5.2	2.7	89.9	70.5
	15	5.0	2.5	2.05	1200	1.25	0.458	4.8	109.6	58.6	1.81	4.8	3.2	90.7	73.5
5(9)	16	1.0	10	0.36	600	1.27	0.932	14	N.O.[j]	55.8	1.82	13	3.2	82.4	50.5
	17	2.0	5.1	0.76	1200	1.21	0.444	6.2	N.O.[j]	57.1	2.23	8.8	2.9	86.1	60.3
	18	3.0	2.6	1.18	1200	1.01	0.370	6.5	105.8	59.3	1.97	6.8	3.2	87.9	65.9
	19	4.0	2.6	1.61	1200	1.62	0.594	7.7	106.4	61.2	1.82	5.4	2.6	90.0	70.8
	20	5.0	2.6	2.05	1200	1.56	0.572	5.8	109.7	63.2	1.68	4.3	2.6	89.2	70.2
6(10)	21	1.0	20	0.36	1800	0.25	0.061	0.45	N.O.[j]	66.5	1.95	5.3	2.7	89.6	70.4
	22	2.0	40	0.76	1800	2.09	0.511	0.91	119.4	68.6	2.04	3.2	2.3	92.4	78.1
	23	3.0	60	1.18	1200	3.54	1.30	0.99	124.5	71.2	1.88	2.9	2.8	91.6	77.5
	24	4.0	60	1.61	1800	6	1.47	0.82	130.0	73.3	1.87	2.1	2.3	93.6	82.1
	25	5.0	20	2.05	1800	2.92	0.714	0.94	127.2	70.8	1.86	2.2	2.5	93.0	80.8

[a] In 54 mL of toluene. [b] See ref 37a. [c] After workup (see Experimental Section). [d] As calculated from polymerization yield. [e] As calculated from $v_{p,apparent}$. [f] Determined from GPC analysis relative to polystyrene standards; polydispersity index = M_w/M_n. [g] Determined from polymer ^{13}C NMR pentad analysis. [h] fractional dyad content, $r = (\Sigma_{x,y}\, xmry + \Sigma_{x,y}\, xrmy + 2\Sigma_{x,y}\, xrry)/2$, with $x, y \in \{r, m\}$. [i] Calculated *rrrr* signal integral; see Supporting Information for experimental and calculated pentad distributions. [j] Not observed.

proposed rate laws that differ in their [propylene] dependence.[11,38] This approach is used for analyzing product molecular weight and the abundance of *m* and *mm* stereodefects, always against the background of chain propagation, reasonably assumed to be first-order in monomer.[39] The present work reveals that these effects are particularly sensitive to counteranion identity.

Limited, but anion-dependent increases in product molecular weights (Table 8) are observed with increasing monomer pressure, arguing that [monomer]-dependent termination processes are significant.[11,38] The sensitivity of M_n to propylene pressure change is markedly higher in the $MeB(C_6F_5)_3^-$ polymerization system (**7**), suggesting that the ratio of rates for unimolecular termination (v_{t1}) vs [monomer]-dependent termination ($v_{t2,propylene}$) is higher in this case.[17] This is illustrated in Figure 7: assuming negligible chain transfer involving species other than propylene, the slope and intercept from a linear fit

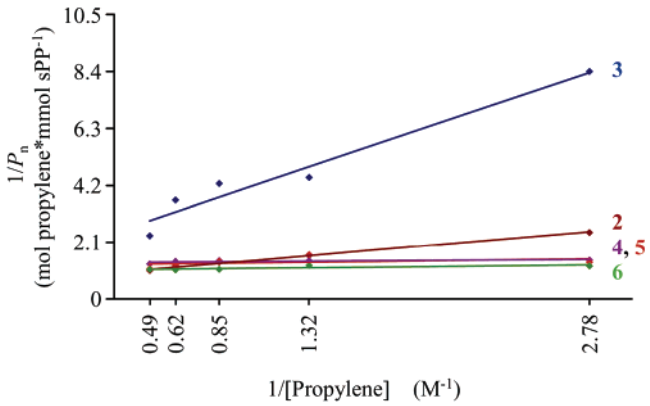

Figure 7. Product $1/P_n$ at 60 °C plotted vs 1/[propylene] for **1**+ indicated cocatalysts (Table 8).

of $1/P_n$ vs. 1/[propylene] (P_n is the number-average degree of polymerization; see eq 9) are equal to k_{t1}/k_p, and $k_{t2,propyene}/k_p$

$$\frac{1}{P_n} = \frac{v_{t2,propylene} + v_{t1}}{v_p} = \frac{k_{t2,propylene}}{k_p} + \frac{k_{t1}}{k_p}\left(\frac{1}{[propylene]}\right) \quad (9)$$

respectively (v_p being the rate of polymerization, assumed to be first-order in [propylene]).[17] The other catalyst-cocatalyst systems studied here, including MAO (**2**, for which chain transfer to aluminum alkyls cannot be ruled out), are indistinguishable in this respect, in particular exhibiting a general suppression of unimolecular termination (Figure 7). However, the variance in GPC-determined M_w values propagates to substantial uncertainties in the quantitation of k_{t1}/k_p, and $k_{t2,prp}/k_p$.[11c1]H NMR end-group analysis of the product polymers reveals that in these systems, 2,1-misinsertion followed by β-hydrogen transfer to Zr is not significant (less than 10%),[40]

(38) (a) For C_s-symmetric catalysts, lower propylene concentrations correlate with lower product molecular weights and tacticities (mostly *m* stereodefects), ref 13c. (b) In contrast, declining isotacticity with increasing monomer concentration is observed in C_1-symmetric catalysts: Kukral, J.; Lehmus, P.; Feifel, T.; Troll, C.; Rieger, B. *Organometallics* **2000**, *19*, 3767−3775. (c) For C_2-symmetric catalyst propylene concentration studies, see ref 17, and also: (d) Busico, V.; Cipullo, R.; Cutillo, F.; Vacatello, M. *Macromolecules* **2002**, *35*, 349−354, (e) Busico, V.; Brita, D.; Caporaso, L.; Cipullo, R.; Vacatello, M. *Macromolecules* **1997**, *30*, 3971−3977, and (f) Resconi, L.; Fait, A.; Piemontesi, F.; Colonesi, M. *Macromolecules* **1995**, *28*, 6667−6676.

(39) Examination of insertion rate vs propylene concentration from Table 8 reveals an approximately linear correlation in several systems, thus insertion is assumed to be first-order in monomer in the present model. This was also observed for the polymerization of 1-hexene catalyzed by [*rac*-(C_2H_4-(1-indenyl)$_2$)ZrMe] [$MeB(C_6F_5)_3$] over the temperature range of −10 °C to 50 °C, see ref 40. However, for C_2-symmetric catalyst propylene studies, there is debate in the literature as to the exact order of monomer in production of isotactic polypropylene. See refs 17, 38d−f. Ref 38d contains a model reconciling observed apparent propagation [propylene] dependences using a rigorous approach that holds propagation to be first-order in monomer.

also arguing that chain transfer to monomer is the preferred bimolecular termination route, in these systems.

Increased monomer concentrations are accompanied by increases in syndiotacticity in all systems studied (Figure 6). Statistical techniques for modeling polymer ^{13}C NMR pentad distributions have been described for C_s-symmetric catalyst systems, in particular for simultaneous estimation of probabilities (relative to propagation) for events that produce *m* steric dyads and *mm* steric triads in the product polymer.[13] These models have the advantage of accounting for steric pentads (or any *n*-ads) containing multiple stereodefects ('shared pentads' e.g. *mrmr*, or *mmrm*). We apply here a standard statistical model[13c,d] to extract the probability P_{mm} of *mm*-generating processes and P_m of *m*-generating processes, that takes into account their contributions to shared pentad intensity. This model is based on the assumption of perfect enantiomorphic site control, as has been justified in several previous examples for this class of catalysts.[13] Experimental and calculated pentad distributions for both pressure- and temperature-dependence polymerization series appear in the Supporting Information.

Catalyst site epimerization, having the proposed rate law, $\upsilon_{se} = k_{se}$[catalyst], leads to the formation of *m* steric dyads as stereodefects in the product polymer when followed by "normal" chain-migratory insertion, but *is not necessarily* the most significant factor in degradation of syndiotacticity at the temperature maintained for this set of experiments (60 °C). In another possible scenario, β-hydrogen transfer to the catalyst metal center is followed by *re*−*si* interconversion of the resulting π-macroolefin complex, and reinsertion (chain epimerization, Scheme 1E). Concomitant stereoinversion at the metal (ion-pair reorganization, Scheme 1E, pathway i) also generates an *m* stereodefect. This process would then have the same stereosequence *and* rate law as site epimerization. It is possible that in certain systems, ion-pair reorganization of the π-macroolefin complex proceeds rapidly compared to the reinsertion step (the macroolefin being 1,1′-disubstituted). Chain epimerization without stereoinversion of the metal generates an *mm* stereodefect (Scheme 1E, pathway ii).[11a,11c,41] As Busico et al. have recently observed,[2a] *m* stereodefects can in principle also arise from insertion without chain migration ("back-side attack," opposite the anion, rather than same-side attack). In fact, any 1,2-insertion in which no net stereochemical inversion of the catalyst occurs, if followed by a "normal" chain-migratory insertion, will give rise to an isolated *m* stereodefect, either as an *mrr* or *rmr* tetrad, depending on the enantiofacial orientation of the back-side misinserted monomer (Scheme 1D). If we assume $\upsilon_{bsa} = k_{bsa}$[catalyst][propylene] for such a process, then the *m* stereodefect probability can be expressed as in eq 10.

$$P_m = \frac{\nu_{bsa} + \nu_{se}}{\nu_p} = \frac{k_{bsa}}{k_p} + \frac{k_{se}}{k_p}\left(\frac{1}{[\text{propylene}]}\right) \qquad (10)$$

A linear fit of P_m vs 1/[propylene] then gives estimates for k_{bsa}/k_p and k_{se}/k_p (as intercept and slope, respectively, eq 10; see Figure 8, Table 9). In this and subsequent models, υ_p, the rate of polymerization, represents the sum of rates for chain migratory insertion, misinsertion via backside attack, and enantiofacial misinsertion, all assumed to be first order in [propylene]. The present results indicate that k_{bsa} is detectably nonzero at 60 °C with $MeB(C_6F_5)_3^-$ as the anion (**7**, in agreement with ref 2a), and indeed for all activators treated in the present report. The observed anion ordering in k_{se}/k_p is FAl-(2-$C_6F_5C_6F_4)_3^-$ (counteranion in **10**) < $MeMAO^-$ (**2**) < MeB-(2-$C_6F_5C_6F_4)_3^-$ (**8**) < $B(C_6F_5)_4^-$ (**9**) < $MeB(C_6F_5)_3^-$ (**7**). This ordering does not track ion pairing strength, but there is no reason to expect it should:[2a,b] it is possible that ion pairing dynamics and counteranion structure/electronics influence the propagation and site epimerization processes to different degrees. The anion ordering in k_{bsa}/k_p, **10** ∼ 2 < **9** ∼ **8** < **7**, also fails to adhere to a specific trend.

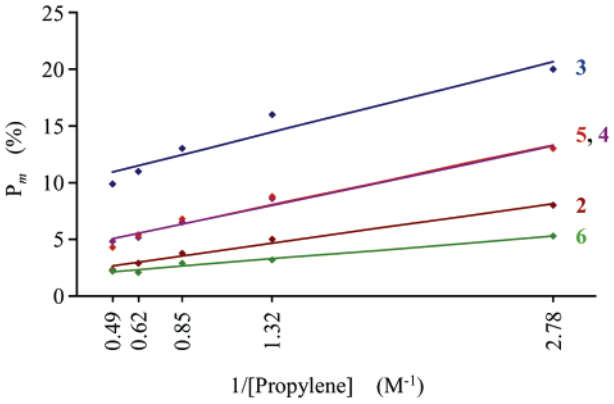

Figure 8. Product P_m at 60 °C plotted vs 1/[propylene] for **1**+ indicated cocatalysts (Table 8).

Table 9. Slopes, Intercepts, and Rate Ratios (%) of *m* Stereodefects Originating from Site Epimerization vs "Back-Side" Misinsertion Obtained from P_m vs 1/[Propylene] Plots for Polymerizations Mediated by **1**+ Indicated Cocatalysts under 1.0−5.0 atm Propylene at 60 °C[a]

cocat. (cat)	k_{se}/k_p[b] (slope)	k_{bsa}/k_p[b] (intercept)	υ_{se}/υ_p[c]	$\upsilon_{sc}/\upsilon_{sc} + \upsilon_{bsa}$[c]
2	0.0243(19)	0.0146(28)	0.067	0.82
3(7)	0.0442(62)	0.0863(90)	0.12	0.58
4(8)	0.034(29)	0.034(43)	0.1	0.76
5(9)	0.0374(37)	0.0319(55)	0.093	0.73
6(10)	0.0141(12)	0.0144(18)	0.039	0.73

[a] Confidence intervals presented at the 90% confidence level. [b] k_p, k_{se}, and k_{bsa} are as defined in eq 10. [c] At 60 °C, 1.0 atm, [propylene] = 0.364 M, see ref 37a for conversion. $\upsilon_{se}/\upsilon_p = (k_{se}/k_p)$ *(1/[propylene]); $\upsilon_{se}/(\upsilon_{se} + \upsilon_{bsa})$ represents the fraction of *m* stereodefects attributable to site epimerization at 60 °C, 1.0 atm.

This analysis employs the assumptions that backside attack and site epimerization occur according to the above rate laws and are the *only* processes giving rise to *m* stereodefects. Independent evidence supporting a backside reaction pathway is desired. Also, structure/function relationships are meaningful only when determined for elementary processes; the product polymer features analyzed herein are each derivative phenomena. Estimates for k_p using available activity data are required to extract approximate values for k_{se} and k_{bsa}; the results of this analysis, along with a discussion of its inherent limitations, are presented below.

The decrease in *m* stereodefect abundance with increasing monomer concentration is found here to be greater than that of the *mm* stereodefect abundance, this latter decline being largest with $MeB(C_6F_5)_3^-$ system but undetectable for the FAl(2-$C_6F_5C_6F_4)_3^-$-derived catalyst **10**. Rate constants for chain epimerization ($\upsilon_{ce} = k_{ce}$[catalyst]) and enantiofacial misinsertion

(40) Liu, Z.; Somsook, E.; White, C. B.; Rosaaen, K. A.; Landis, C. R. *J. Am. Chem. Soc.* **2001**, *123*, 11 193−11 207.
(41) Sillars, D. R.; Landis, C. R. *J. Am. Chem. Soc.* **2003**, *125*, 9894−9895.

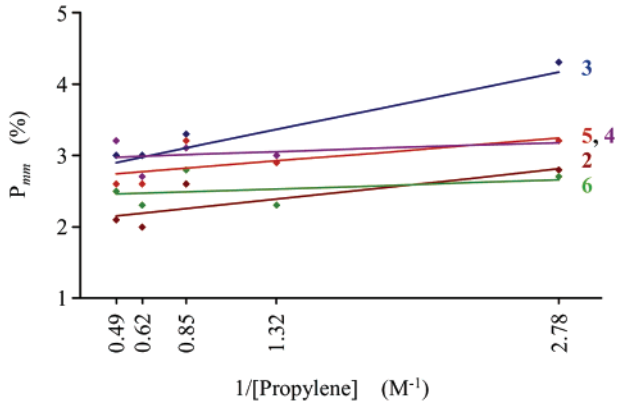

Figure 9. Product P_{mm} at 60 °C plotted vs 1/[propylene] for **1**+ indicated cocatalysts (Table 8).

Table 10. Slopes, Intercepts, and Rate Ratios (%) of *mm* Stereodefects Originating from Chain Epimerization vs Enantiofacial Misinsertion Obtained from P_{mm} vs 1/[Propylene] Plots for Polymerizations Mediated by **1**+ Indicated Cocatalysts under 1.0−5.0 atm Propylene at 60 °C[c]

cocat. (cat)	k_{ce}/k_p[b] (slope)	k_{em}/k_p[b] (intercept)	v_{ce}/v_p[c]	$v_{ce}/v_{ce}+v_{em}$[c]
2	0.0026(13)	0.0204(20)	0.0071	0.26
3(7)	0.0057(18)	0.026(26)	0.016	0.38
4(8)	0.0009(11)	0.0291(17)	0.0063	0.19
5(9)	0.0023(14)	0.0261(20)	0.0025	0.078
6(10)	0.0009(13)	0.0239(19)	0.0025	0.094

[a] Confidence intervals presented at the 90% confidence level. [b] k_p, k_{ce}, and k_{em} are as defined in eq 11. [c] At 60 °C, 1.0 atm, [propylene] = 0.364 M, see ref 37a for conversion. $v_{ce}/v_p = (k_{ce}/k_p) * (1/[\text{propylene}])$; $v_{ce}/(v_{ce} + v_{em})$ represents the fraction of *mm* stereodefects attributable to site epimerization at 60°C, 1.0 atm.

($v_{em} = k_{em}$[catalyst][propylene]) vs propagation can be calculated from P_{mm} for each catalyst (eq 11, with v_p as defined above), by analyzing the plots of P_{mm} vs 1/[propylene] for each system (Figure 9, Table 10). The present collected results

$$P_{mm} = \frac{v_{em} + v_{ce}}{v_p} = \frac{k_{em}}{k_p} + \frac{k_{ce}}{k_p}\left(\frac{1}{[\text{propylene}]}\right) \qquad (11)$$

suggest that enantiofacial misinsertion is the prevailing process for the generation of *mm* stereodefects in all systems studied here. Similar evaluation of the data for $(1,2\text{-SiMe}_2)_2\{C_5H_2\text{–}4\text{-R}\}\{C_5H\text{-}3,5\text{-}(CHMe_2)_2\}ZrCl_2$ (R = H, $CHMe_2$, $SiMe_3$) activated by MAO at 24 °C suggests that in this case,[11c] the relative contribution of enantiofacial misinsertion is small. This distinction is likely due to metallocene structural differences, and possibly also to differences in reaction temperature.

C. Anion Mobility during Propylene Polymerization Probed in Situ by Enchainment Syndioselection. Considering the large observed counteranion effects on M_w, *m*, and *mm* stereodefects, it is important to inquire into their origin;[42] as indicated above, counteranion effects, or any effects, are best analyzed against the rates for individual processes. However, use of polymerization analytical yields for determination of k_p values, necessary for determination of k_{se}, k_{bsa}, k_{ce}, and k_{em}, can be relied on only in certain cases. Propagation rates are systematically underrepresented owing to reversible and irreversible catalyst deactivation and catalyst induction, each of which is likely both cocatalyst- and temperature-dependent.[43] Correcting for such effects would have the effect of inflating $k_{p,apparent}$, thus increasing the estimates for elementary rate constants k_{se}, k_{bsa}, k_{ce}, and k_{em} from the relative quantities derived using eqs 10 and 11. However, reaction of catalysts with adventitious stoichiometric poisons can be reasonably assumed to proceed to completion in all cases. Thus the depression of $v_{p,apparent}$ due to unintentional contamination should be statistical and independent of catalyst and temperature, and can be safely ignored when comparing $k_{p,apparent}$ among the present catalyst systems, with the exception of **1** + **2**, wherein large quantities of excess alkylaluminoxanes introduce a further systematic uncertainty. Catalyst thermal decomposition is clearly both temperature- and catalyst-dependent (and possibly also [catalyst]-dependent), and will thus introduce systematic errors into estimates of the elementary rate constants k_{se}, k_{bsa}, k_{ce}, and k_{em} for each system. However, we observe that greater polymerization rates ($v_{p,apparent}$, see Table 7) are generally associated with greater thermal instability, thus suggesting a greater underrepresentation of these elementary rate constants with systems that are more active.[44] It has been observed by Landis et al. that the fraction of catalytically active states in isospecific 1-hexene polymerizations is moderately higher with $B(C_6F_5)_3$ as activator than with $[PhNH(Me_2)]^+B(C_6F_5)_4^-$, suggesting that the actual propagation rate constant is indeed higher in the latter case. Thus, underrepresentation of rate constants k_{se}, k_{bsa}, k_{ce}, and k_{em} can reasonably be expected to be larger with $B(C_6F_5)_4^-$ than with $MeB(C_6F_5)_3^-$ in the present case. Also, in both cases, the fraction of active catalysts at any given time is approximately the same as the fraction of catalysts that were active at some time, suggesting that the formation of dormant states on the time scale of their experiments (0.01−1000 s) is not significant.[43b] Subsequent direct NMR observation of catalyst polymeryl species has shown that accumulation of dormant states is insignificant.[43d] Assuming this holds in the present systems, the above findings on active site count and activity provide the following condition for comparability: in comparing two catalysts of different activity, if the more active catalyst gives the larger apparent value for some elementary rate constant, the *difference* in this value for the two catalysts is thus underrepresented, and the ordering is reliably given by the data. The ordering can be established, in any comparison for which this condition is satisfied. Estimates for k_p, k_{se}, k_{bsa}, k_{ce}, and k_{em} among the present series of catalysts are summarized in Table 11.[45] Values for k_p at 60 °C were determined by extrapolation of activity Arrhenius plots established from the temperature-

(42) For general kinetic models, see: (a) Nele, M.; Mohammed, M.; Xin, S.; Collins, S.; Dias, M. L.; Pinto, J. C. *Macromolecules* **2001**, *34*, 3830−3841. (b) Grisi, F.; Longo, P.; Zambelli, A.; Ewen, J. A. *J. Mol. Catal. A: Chem.* **1999**, *140*, 225. (c) Ewen, J. A. *J. Mol. Catal. A: Chem.* **1998**, *128*, 103.

(43) Whereas the thermal instability of group IV metallocenium salts of $B(C_6F_5)_4^-$ is well-known (refs 1b,2,7c) previous work (ref 7c) indicates that $B(C_6F_5)_4^-$-based systems are to some degree stabilized in the presence of olefin, and extant literature finds catalyst activity during polymerization to be more or less constant: (a) Wester, T. S.; Johnsen, H.; Kittilsen, P.; Rytter, E. *Makromol. Chem. Phys.* **1998**, *199*, 1989−2004. Negligible catalyst deactivation is observed in 1-hexene polymerizations using [*rac*-$C_2H_4(indenyl)_2ZrMe][MeB(C_6F_5)_3]$, see: (b) Liu, Z.; Somsook, E.; Landis, C. R. *J. Am. Chem. Soc.* **2001**, *123*, 2915−2916. For relevant ethylene homopolymerization results using mononuclear and binuclear constrained geometry catalysts see: (c) Abramo, G. P.; Li, L.; Marks, T. J. *J. Am. Chem. Soc.* **2002**, *124*, 13 966−13 967, and also see ref 2c. (d) Landis, C. R.; Rosaaen, K. A.; Sillars, D. R. *J. Am. Chem. Soc.* **2003**, *125*, 1710−1711.

(44) For example, in NMR study of the freshly generated ion pairs, we observe systems **8** and **9** to undergo rapid decomposition (with **9** faster than **8**), while **7** decomposes slowly and **10** exhibits comparatively high thermal stability.

Table 11. Estimated Absolute Rate Constants for Propagation, Site Epimerization, "Back-Side" Misinsertion, Chain Epimerization, and Enantiofacial Misinsertion Obtained from Activities, P_m vs 1/[Propylene] Plots, and P_{mm} vs 1/[Propylene] Plots for Polymerizations Mediated by **1**+ Indicated Cocatalysts under 1.0−5.0 atm Propylene at 60 °C[a]

cocat. (cat)	k_p[b] ($M^{-1}*s^{-1}$)	k_{se}[c] (s^{-1})	k_{bsa}[c] ($M^{-1}*s^{-1}$)	k_{ce}[d] (s^{-1})	k_{em}[d] ($M^{-1}*s^{-1}$)
2	402(44)	9.8(13)	5.9(13)	1.04(55)	8.2(12)
3(7)	41.8(8)	1.85(26)	3.61(38)	0.239(75)	1.09(11)
4(8)	321(12)	10.9(10)	10.9(14)	0.29(37)	9.36(65)
5(9)	297(4)	11.1(11)	9.5(16)	0.69(42)	7.75(62)
6(10)	33.7(16)	0.474(47)	0.486(65)	0.03(44)	0.807(74)

[a] Confidence intervals presented at the 90% confidence level; k_p, k_{se}, k_{bsa}, k_{ce}, and k_{em} as defined in eqs 10 and 11. [b] k_p values are extrapolated from plots of $\ln(k_{p,apparent})$ vs. $1/T$ (see text). [c] From plots using eq 10. [d] From plots using eq 11.

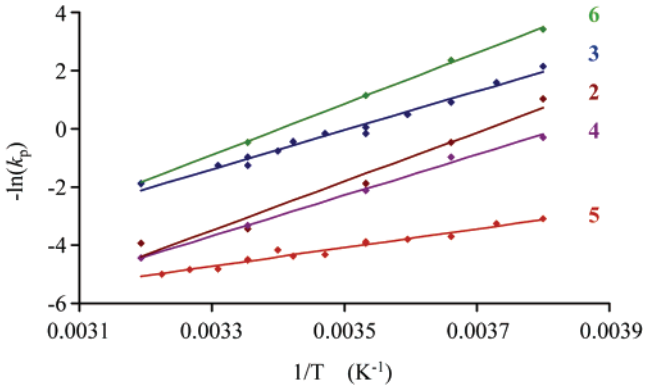

Figure 10. Plots of $-\ln(k_p)$ vs. 1/(polymerization temperature) for **1**+ indicated cocatalysts under 1.0 atm propylene over the temperature range from −10° to +60 °C in toluene (Table 7; k_p values corrected for [propylene] temperature dependence).

dependence data (Figure 10), excluding experiments in which k_p is obviously underrepresented by $k_{p,apparent}$ (see Table 7). Confidence intervals for these projected k_p values are given at the 90% confidence level, as determined from linear regression analysis of $\ln(k_{p,apparent})$ vs $1/T$ for each system. Confidence intervals for k_{se}/k_p and k_{bsa}/k_p were determined from linear regression analysis of P_m vs 1/[propylene], and for k_{ce}/k_p and k_{em}/k_p, from P_{mm} vs 1/[propylene]; these are also given at the 90% confidence level. Confidence intervals for k_{se}, k_{bsa}, k_{ce}, and k_{em} are derived from those of the parent quantities. Due to the presence of large excesses of aluminoxanes in reactions using **2** as cocatalyst, and the large confidence interval associated with k_p for this system (402(44) s^{-1}) these data are excluded from the present discussion. Also, lack of detailed information on the structure(s) of the catalyst system obtained using this cocatalyst impedes interpretation of rate data from a mechanistic standpoint; data for **2** are presented for consideration in Table 11.

The trends in propagation and site epimerization rates both track ion pairing strength. For k_p (L mol^{-1} s^{-1}), the observed anion ordering is as follows: $FAl(2\text{-}C_6F_5C_6F_4)_3^-$ (**10**, 33.7(16)) < $MeB(C_6F_5)_3^-$ (**7**, 41.8(8)) ≪ $B(C_6F_5)_4^-$ (**9**, 297(4)) < $MeB(2\text{-}C_6F_5C_6F_4)_3^-$ (**8**, 321(12)). For k_{se} (s^{-1}), the ordering is the same: **10** (0.474(47)) < **7** (1.85(26)) ≪ **8** (10.9(10)) ≈ **9** (11.1(11)). These general trends are consistent with the anion coordinating metrics developed on the basis of dynamic NMR-derived ion pair reorganization barriers and anion displacement equilibria.[1b,4a,7c,8a,12] Surprisingly, the observed trend in k_{bsa} (L mol^{-1} s^{-1}) also tracks ion pairing strength: $FAl(2\text{-}C_6F_5C_6F_4)_3^-$ (**10**, 0.486(65)) < $MeB(C_6F_5)_3^-$ (**7**, 3.61(38)) < $B(C_6F_5)_4^-$ (**9**, 9.5(16)) ≈ $MeB(2\text{-}C_6F_5C_6F_4)_3^-$ (**8**, 10.9(14) s^{-1}). If this trend accurately reflects selectivity for same-side approach of the olefin with respect to the counteranion, it seems counterintuitive from the standpoint of steric factors: certainly a more intimately bound anion would be more likely to suppress same-side attack. However, it is possible that a strongly coordinating anion stabilizes the distribution of positive charge at the catalyst metal center such that same side attack (as with "normal" chain-migratory insertion) is favored.[28] Considering that anion stereochemical mobility, catalyst stability, and reactivity all seem to depend strongly on the coordinative contribution to the cation−anion interaction, it seems likely that charge distribution and stabilization of the cationic moiety is highly anion-dependent, and that the anion is intimately involved in the insertion reaction (and in competing processes). The formal charge of the cationic olefin π-adduct fragment (assuming one exists) is the same as the isolated catalyst, and it is likely that such species also persist as contact ion pairs in solution.[28] Interaction between the anion and a π-adduct may indeed *involve* the olefin (inasmuch as the anion's charge is itself localized), the anion possibly assisting in olefin activation.[24] This would explain the remarkable fact that the fluoroaluminate system yields polymer at all, given the remarkable kinetic inertness of the anion as a ligand in this system. Further evidence of ion pairing influences can be seen in the trend in enantiofacial misinsertion (k_{em}, L mol^{-1} s^{-1}), with **10** (0.807(74)) < **7** (1.09(11)) ≪ **9** (7.75(62)) < **8** (9.36(65)). This trend in particular suggests a complex dependence on both electronic and steric factors.

Chain epimerization is observable in all systems with the notable exception of catalyst system **10** (k_{ce} = 0.03(44), indistinguishable from zero, as with **8**, having k_{ce} = 0.29(37), a rather large confidence interval; see Table 11) and is also suppressed, but to a lesser extent, with **7** (k_{ce} = 0.239(75)).[46] Conversely, the weakly coordinating $B(C_6F_5)_4^-$ exhibits a chain epimerization rate constant of 0.69(42), ∼20× greater than that of the $FAl(2\text{-}C_6F_5C_6F_4)_3^-$ anion (although indistinguishable from **10** at the 90% confidence level). The diminished chain epimerization channel observed with **10**, if well-represented by the present data, is possibly due to suppression of β-hydrogen transfer to Zr (Scheme 1E). A tightly bound counteranion would a priori be expected to destabilize the 4-center transition state generally considered necessary for β-hydrogen transfer (termination via β-hydrogen transfer is undetectable with **10**, but also with **8** and **9**).[11a,41] This possibility is not inconsistent with (but by no means conclusively demonstrates) the ideas of: (i) intimate involvement of the counteranion in polymerization events, and (ii) multiple available, counteranion-differentiated pathways for monomer activation and enchainment.

The above observed trends mirror ion pairing strength quite well, and since these orderings arise from estimates of k_p, which

(45) See Table 1 in Supporting Information for additional polymerization results used together with those in Table 7 to generate rate constants k_p for Table 11.

(46) Absolute rates for chain epimerization and enantiofacial misinsertion for each catalyst at each pressure can be roughly gauged using eq 11 (P_{mm}) and insertion rates. The chain epimerization rates follow the ordering: **3** > **5** > **2** > **4** > **6**. It is likely in any event that the various steps involved in chain epimerization are subject to anion-dependent steric and electronic influences in a complex manner.

Table 12. Propylene Polymerization Results for the Reactions Mediated by **1**+ Indicated Cocatalysts in 1,3-Dichlorobenzene[a] or Octane[a] under 1.0 atm of Propylene at 25 °C

solvent[a]	exp. no.	cocat. (cat.)	cat. (μmol)	time (s)	yield[b] (g)	activity[c] ($\times 10^6$)	T_m (°C)	M_w[d] (kg*mol^{-1})	P.D.I.[d]	*rmmr*[e] (%)	*mmrr*[e] (%)	*rrmr*[e] (%)	*rrrr*[e] (%)
1,3-dichloro-benzene	1	2	2.5	120	0.56	6.5	N.O.[f]	110	1.85	1.6	4.3	18	49
	2	3(7)	10	360	2.67	2.67	113.8	97.6	1.76	2.3	4.6	17	49
	3	4(8)	3.8	900	0.82	0.86	122.2	93.3	2.24	2.4	4.4	17	50
	4	5(9)	8.0	120	1.21	4.53	125.4	104	1.92	2.3	4.3	17	50
	5	6(10)	10	900	2.4	0.96	131.6	127	1.78	2.3	4.3	17	50
octane	6	2	3.6	600	0.83	1.4	N.O.[f]	147	1.86	1.3	2.8	3.4	85
	7	3(7)	20	9000	3.16	0.063	N.O.[f]	49.7	2.01	1.6	3.4	10	69
	8	4(8)	5.0	1200	2.09	1.256	N.O.[f]	104	1.82	1.9	4.0	6.5	77
	9	5(9)	10	1800	2.45	0.49	N.O.[f]	139	1.83	1.5	3.2	4.9	82
	10	6(10)	40	1500	2.47	0.148	N.O.[f]	154	1.89	1.4	2.8	1.9	89

[a] 50 mL, 4 mL toluene injected with catalyst solution. [b] After workup (see Experimental Section). [c] Units: g polymer/(mol cat.*atm*h). [d] Determined from GPC analysis relative to polystyrene standards; polydispersity index = M_w/M_n. [e] Pentad integrals from polymer ^{13}C NMR. [f] Not observed.

we also observe to track ion pairing strength, it is worthwhile to entertain the possibility that errors in the k_p estimates, rather than systematic chemical structure/function relationships, dominate the analysis. The present findings, if valid, do shed light on some interesting observations[10] that have also received attention in recent literature:[2a,b] for example, $B(C_6F_5)_4^-$ (**9**) is found to produce a higher-syndiotacticity polymer than $MeB(C_6F_5)_3^-$ (**7**) at all temperatures, even though it is thought to be more weakly bound to the cation. At [propylene] = 0.36 M (1 atm. system pressure, T = 60 °C), the present results give $P_{m,7}/P_{m,9}$ ranging from 1.5 to 2.8, as determined directly from NMR analysis of the product polymers from these two catalysts. The aforementioned observations are consistent with a scenario in which $P_{m,7}/P_{m,9} < \upsilon_{p,9}/\upsilon_{p,7}$ (see eq 10 above). Thus at 25 °C, for example, relative insertion rates $\upsilon_{p,9}/\upsilon_{p,7} > 2.8$ would give $\upsilon_{m,9} > \upsilon_{m,7}$, as expected ($P_m \times \upsilon_p = \upsilon_m = \upsilon_{bsa} + \upsilon_{se}$). In such a scenario, *m* stereodefect generation proceeds more rapidly in **9** than **7**, but by a smaller margin than propagation. In fact, activity measurements give an estimated $\upsilon_{p,9}/\upsilon_{p,7}$ = 25.9(79), at 25 °C, suggesting that this is indeed the case. A similar argument explains comparative polymer M_w values: whereas attenuated β-hydrogen elimination with $MeB(C_6F_5)_3^-$ and FAl-(2-$C_6F_5C_6F_4$)$_3^-$ does contribute to increased polymer M_w values, $B(C_6F_5)_4^-$ produces a higher M_w product due to its much greater propagation rate.

D. Solvent Effects on Polymerization Stereocontrol. In nonpolar hydrocarbon solvents such as toluene (ϵ = 2.15), which are commonly used for olefin polymerization, strong cation−anion interactions[12] are doubtless an important modulator of reactivity in the present class of catalysts.[2]

To probe the effects of polar solvation-induced ion pair weakening on enchainment stereochemistry, polymerizations were also carried out in more polar 1,3-dichlorobenzene (ϵ = 5.04; Table 12). The net result is dramatic compression in the dispersion of polymerization rates and collapse of *rrrr*, *m*, and *mm* stereosequence percentages to the experimentally indistinguishable values of 50%, 17.5%, and 4%, respectively, for all cocatalysts studied, indicating that polar solvents significantly weaken ion pairing effects on stereocontrol in this system (Figure 11).[47] In contrast, polymerizations in less polar octane (ϵ = 2.08; Table 12) evidence trends similar to those in toluene, but with more dramatic decreases in polymerization activity and slightly lower to negligible changes in product syndiotacticities. Although stronger ion pairing effects in octane vs toluene can be used to explain the observed decrease in activity in **9** and **10** (95% and 25% respectively), the lower solubility of these

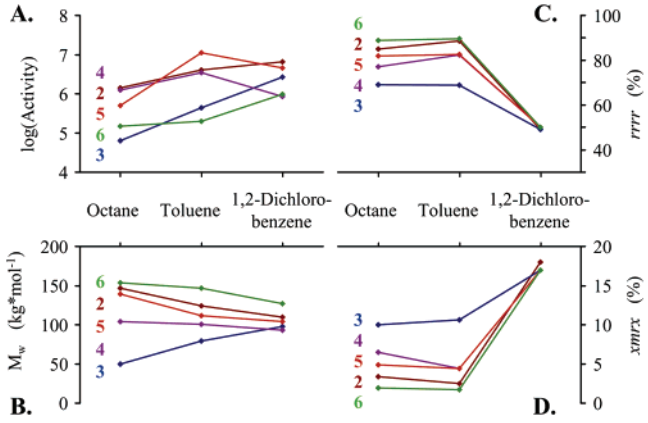

Figure 11. A. log(polymerization activity), B. Polypropylene M_w, C. *rrrr* pentad intensity (%), and D. *xmrx* pentad intensity (%) data for polypropylenes produced by **1**+ indicated cocatalysts under 1.0 atm of propylene at 25 °C in octane, toluene, and 1,3-dichlorobenzene solutions.

ion pair complexes in octane is a tenable explanation for the reduced productivity.[43a]

E. Catalyst Concentration and Added Li^+ $MeB(C_6F_5)_3^-$ Effects on Syndiospecific Polymerizations Mediated by 7. Increased zirconocenium ion pair concentrations and the addition of Li^+ $MeB(C_6F_5)_3^-$ (**11**) have recently been reported to accelerate anion exchange/catalyst symmetrization processes (cf., eq 2).[14] An ion quadruple (**K**) or higher aggregate was proposed to be the key intermediate in such acceleration. To test the possible effects of putative ion pair aggregation and the introduction of lithium counteranion salts on the present polymerization system, experiments in which the concentration of **7** was varied, and experiments examining the effect of added Li^+ $MeB(C_6F_5)_3^-$ on propylene polymerizations catalyzed by **1** + **3**, were carried out. A priori, structures such as **K** might be expected to exhibit enhanced degrees of stereochemical mobility, which would consequently erode product syndiotacticity. Indeed, evidence for[14] and against[12,14] increased catalyst

(47) (a) Propylene solubilities at 1 atm can be expected to vary somewhat with solvent. However, with 1,3-dichlorobenzene as solvent we observe that whereas activity (hence insertion rate) increases, so also does the rate of *xmrx* steric pentad formation, *relative to insertion*. On the basis of what we have demonstrated here from the propylene concentration study, we would expect the opposite, were the effect exclusively a concentration effect. (b) Herfert, N.; Fink, G. *Makromol. Chem.* **1992**, *193*, 773−778. (c) Coevoet, D.; Cramail, H.; Deffieux, A. *Makromol. Chem. Phys.* **1999**, *200*, 1208−1214. (d) For solvent effects in C_2-symmetric catalyst system, Forlini, F.; Tritto, I.; Locatelli, P.; Sacchi, M. C.; Piemontesi, F. *Makromol. Chem. Phys.* **2000**, *201*, 401−408. (d) For CGC catalyst systems, see: Kleinschmidt, R.; Griebenow, Y.; Fink, G. *J. Mol. Catal. A-Chem.* **2000**, *157*, 83−90.

Table 13. Concentration Effects on Propylene Polymerization Results for the Reactions Mediated by **1**+ $B(C_6F_5)_3$ (**3**) in Toluene under 1.0 atm of Propylene at 25 °C[a]

exp. no.	cat. (μmol)	time (s)	yield[b] (g)	activity[c] ($\times 10^6$)	T_m (°C)	M_w[d] (kg*mol^{-1})	P.D.I.[d]	*rmmr*[e] (%)	*mmrr*[e] (%)	*rrmr*[e] (%)	*rrrr*[e] (%)
1	800	600	4.92	0.37	102.5	56.9	1.66	1.6	3.3	11.0	68.1
2	400	900	2.30	0.46	102.5	66.4	1.7	1.5	3.1	10.5	69.5
3	200	2400	5.90	0.44	101.4	79.4	1.81	1.5	3.1	10.6	69.4
4	100	2400	2.59	0.39	102.5	77.5	1.85	1.6	3.1	10.5	69.6
5	50	3600	0.86	0.17	101.0	76.0	1.78	1.5	3.1	10.8	69.2
6	25	7200	2.10	0.42	101.3	81.9	1.83	1.7	3.2	10.9	68.7

[a] In 104 mL toluene. [b] After workup (see Experimental Section). [c] Units: g polymer/(mol cat.*atm*h). [d] Determined from GPC analysis relative to polystyrene standards; polydispersity index = M_w/M_n. [e] Pentad integrals from ^{13}C NMR.

Table 14. Propylene Polymerization Results for the Reactions Mediated by **1** + **3** with Addition of Li^+ $MeB(C_6F_5)_3^-$ (**11**) in Toluene under 1.0 atm of Propylene at 25 °C[a]

exp. no.	cat. (μmol)	added **11** (μmol)	time (s)	yield[b] (g)	activity[c] ($\times 10^6$)	T_m (°C)	M_w[d] (kg*mol^{-1})	P.D.I.[d]	*rmmr*[e] (%)	*mmrr*[e] (%)	*rrmr*[e] (%)	*rrrr*[e] (%)
1	20	0	2400	5.90	0.44	101.4	79.0	1.81	1.5	3.1	10.6	69.4
2	20	20	2400	2.21	0.17	109.5	84.6	1.78	1.7	3.1	9.2	72
3	20	40	1800	4.02	0.40	108.5	83.6	1.84	1.8	3.3	9.4	70.9
4	20	60	1200	3.45	0.52	114.5	86.6	1.8	1.5	2.9	8	75.6
5	20	80	1200	4.43	0.67	112.2	84.5	1.82	1.6	3	8.9	73.2
6	20	100	1200	4.90	0.74	114.6	93.0	1.84	1.5	2.9	7.8	76

[a] In 104 mL toluene. [b] After workup (see Experimental). [c] Units: g polymer/(mol cat.*atm*h). [d] Determined from GPC analysis relative to polystyrene standards; polydispersity index = M_w/M_n. [e] Pentad integrals from ^{13}C NMR.

K

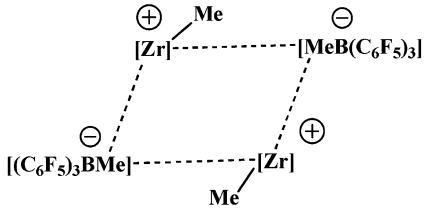

site epimerization rates (eq 2) with increasing catalyst concentration in the absence of olefin has been presented in the literature. However, in the present experiments with **7**, catalyst activity and product syndiotacticity were found to be essentially concentration-invariant over a 32-fold catalyst concentration range, while product M_w data decline only modestly at the highest concentrations (Table 13). These results argue that under typical polymerization conditions, where [catalyst] = 25−800 μM (in contrast with the aggregation experiments, in which [catalyst] = 2−20 mM),[14] inter-ion pair exchange via aggregation is not an important factor influencing activity or enchainment stereochemistry. In work presented elsewhere,[28,48] ion-pair aggregation is shown by cryoscopy and pulsed field gradient spin−echo NMR spectroscopy to be insignificant in benzene or toluene solutions for a broad range of single-site metallocenium $MeB(C_6F_5)_3^-$ or $B(C_6F_5)_4^-$ ion pairs, even at concentrations substantially higher than employed here. Taken together, these findings argue that formation of ion quadruples (**K**) or higher-order aggregates is unlikely to be of importance in the present zirconocene-based catalyst systems for single-site α-olefin polymerization.

Experiments examining the effects of added Li^+ $MeB(C_6F_5)_3^-$ (**11**) on propylene polymerizations catalyzed by **1** + **3** reveal at most a minor increase in product M_w, syndiotacticity, or melting point with increased **11** concentrations over a broad range (Table 14). This observation suggests that under the present conditions, either the ion exchange rate (if exchange occurs at all) is dictated by a slow dissociative step, and is thus invariant with [Li^+ $MeB(C_6F_5)_3^-$], or that exchange occurs associatively but without stereoinversion, i.e., through same-side attack (compare eqs 12a and 12b), as proposed by Brintzinger et al.[49] As in the concentration-dependence studies of **7**, catalyst activity and product syndiotacticity are modestly to negligibly invariant to added Li^+ $MeB(C_6F_5)_3^-$, while product M_w may be more sensitive.

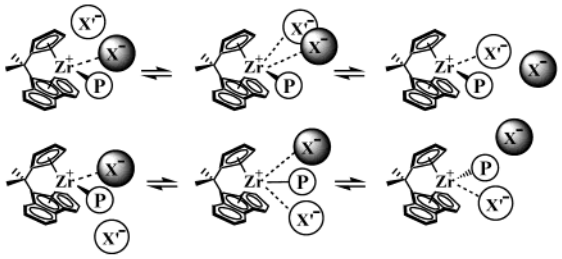

(12a)

(12b)

Conclusions

A series of stable, structurally well-characterized, highly reactive C_s-symmetric zirconocenium ion pair propylene polymerization catalysts has been studied with regard to the molecular and ion pair structure and structural dynamics, both in the solid state and in solution. Ion-pairing differences are evaluated on the basis of detailed spectroscopic/crystallographic characterization and ion pair reorganization/symmetrization kinetics, and reveal strongly anion-dependent correlations with product polypropylene molecular weight and microstructural features. A distinctive signature of the catalyst−cocatalyst interaction emerges: polymerization activity, polymer microstructure, and molecular weight, in particular the relative rates of termination pathways and stereodefect-generating side reac-

(48) (a) Stahl, N. G.; Zuccaccia, C.; Jensen, T. R.; Marks, T. J. *J. Am. Chem. Soc.* **2003**, *125*, 5256−5257. (b) Stahl, N. G.; Marks, T. J.; Macchioni, A.; Zuccaccia, C. Presented in part at the 222nd ACS National Meeting, Chicago, IL, August 2001, Abstract INORG 407.

(49) Li^+ $MeB(C_6F_5)_3^-$ is not assumed to be a solvent-separated or dissociated ion pair.

tions relative to syndiospecific propylene enchainment, are all highly sensitive to the sterics and energetics of cocatalyst binding.

Comparison of solid-state structures demonstrates that the tightly bound $FAl(2\text{-}C_6F_5C_6F_4)_3^-$ counteranion actually draws the $[Me_2C(Cp)(Flu)]ZrMe^+$ Zr center slightly further out of the ligand pocket than does $MeB(C_6F_5)_3^-$. Reciprocal effects on anion structure are larger: differences in flattening of the Group 13 atom geometry and lengthening of the Group 13 atom bond to the bridging moiety with coordination of the anion, demonstrate strong differences in the cation−anion interaction in **7** and **10**. These counteranion differences are further manifested in the rate constants of dynamic unimolecular reorganization processes in isolated $[Me_2C(Cp)(fluorenyl)]ZrMe^+X^-$ ion pairs; from NMR kinetic analysis, we find that the fluoroaluminate ion pair has a far higher barrier to reorganization: $\Delta G^{\ddagger} > 24.8$ kcal/mol vs 21.3(36) kcal/mol for $MeB(C_6F_5)_3^-$ at 127.5 °C. Ion pair reorganization is herein assumed to be kinetically accessible to the metallocene Group 4 olefin polymerization catalysts as a class, but possibly requires the presence of olefin in the fluoroaluminate system (**10**). This is consistent with the commonly accepted chain-swinging model developed in conjunction with metallocene polymerization catalysts for stereoregular propylene polymerization.[11,50]

The above observations and conclusions help reconcile the present accumulated evidence for appreciable counteranion/cocatalyst influences on product polymer features with the complex manifold of processes proposed to be kinetically accessible during polymerization. Stereodefect frequencies and molecular weights examined as a function of polymerization temperature and monomer concentration across the entire cocatalyst series allow quantitation of anion effects on a collection of processes, and by extension, comparison of $FAl(2\text{-}C_6F_5C_6F_4)_3^-$, $MeB(C_6F_5)_3^-$, $B(C_6F_5)_4^-$, $MeB(2\text{-}C_6F_5C_6F_4)_3^-$, and MAO. Comparing $FAl(2\text{-}C_6F_5C_6F_4)_3^-$ and $MeB(C_6F_5)_3^-$, we find that the latter exhibits a greater proclivity toward unimolecular reorganization/symmetrization and termination processes than does the former, suggesting not only that the difference in ion pairing strength persists during polymerization, but that the fluoroaluminate anion suppresses chain transfer more strongly than does the methylborate. The catalytic activities and polymer syndiotacticities exhibited by $MeB(2\text{-}C_6F_5C_6F_4)_3^-$ lie between those of $MeB(C_6F_5)_3^-$ and $B(C_6F_5)_4^-$, in accord with previous evidence suggesting that, as compared with the former, the bulkier ancillary structure of $MeB(2\text{-}C_6F_5C_6F_4)_3^-$ reduces the ion pairing interactions, all else being equal. However, due to its tendency to form $[Zr-(\mu\text{-}Me)-Zr]^+$ structures, the latter system is more complex. It is evident, however, that the $B(C_6F_5)_4^-$ counteranion is the most weakly bound, exhibiting the most rapid production of *m* and *mm* stereodefects, and by a greater margin, the most rapid chain propagation. Consistently across the present series, polymerization activity decreases and the rate of catalyst site epimerization decreases, as the ion pairing strength is increased. Estimation of absolute rates for propagation, site epimerization, backside misinsertion, enantiofacial misinsertion, and chain epimerization for each of these cation−anion systems provides a complete and self-consistent explanation of the relative syndiotacticities of product polymers from each system. Spectroscopic, theoretical,[24,51] and polymerization studies argue that polar solvents significantly weaken ion pairing, and in accord with a picture in which ion pairing modulates syndiospecific enchainment, we find here that differential anion effects on propagation rates diminish and those on stereodefects *completely vanish* in a more polar solvent. While the present results serve to elucidate the importance of catalyst−cocatalyst interactions in the production of syndiotactic polypropylene,[52] they also reveal a unique new feature of the $FAl(2\text{-}C_6F_5C_6F_4)_3^-$ counteranion. This remarkable species, showing the greatest affinity for the cationic zirconocenium fragment, exhibits the highest, least temperature-dependent syndioselectivity. This unprecedented, cocatalyst-derived stabilization suggests completely new strategies for selectivity enhancement in single-site polymerization processes.

Acknowledgment. Financial support by DOE (DE-FG02-86ER1351) is gratefully acknowledged. M.-C. C. thanks Dow Chemical for a postdoctoral fellowship and Dr. P. Nickias of Dow for GPC measurements. We also thank Dr. L. Li, Dr. H. Ahn, Dr. C. Zuccaccia, Dr. T. R. Jensen, and Mr. N. G. Stahl for helpful discussions.

Supporting Information Available: Complete X-ray experimental details and tables of bond lengths, angles, and positional parameters for the crystal structures of **7** and **10**, additional polymerization results as an extension to results in Table 11 above, and a full-page, low peak-threshold EXSY spectrum for **10** at 127.5 °C, $\tau_m = 800$ ms (15 pages, print/PDF). This material is available free of charge via the Internet at http://pubs.acs.org.

JA036288K

(50) (a) Cossee, P. *Tetrahedron Lett.* **1960**, *17*, 12. (b) Cossee, P. *Tetrahedron Lett.* **1960**, *17*, 17. (c) Arlman, E. J.; Cossee, P. *J. Catal.* **1964**, *3*, 99. Cossee, P. *J. Catal.* **1964**, *3*, 80. Cossee, P.

(51) (a) Beswick, C. L.; Marks, T. J. *Organometallics* **1999**, *18*, 2410−2412. (b) Deck, P. A.; Beswick, C. L.; Marks, T. J. *J. Am. Chem. Soc.* **1998**, *120*, 12 167−12 167. (c) and also see ref. 12.

(52) Chen, M.-C.; Roberts, J. A. S.; Marks, T. J. *Organometallics* **2004**, *23*, 932−935.